

Chapter 2

Signal Processing Model of Human Auditory System

Abstract To evaluate environmental noise, we need to use methods based on functioning of our auditory system. In this chapter, basics of human auditory system are described. First, the ear sensitivity of the human ear from a sound source to the auditory system consisting of the external canal, eardrum, bone chain with oval window, auditory nerve, cochlear nucleus, thalamus, brain stem, and cortex, and signal processing model for evaluation of environmental noise are described. Second, brain responses in relation to basic perception such as loudness and annoyance are described.

Keywords Auditory system • Autocorrelation model • Interaural cross-correlation model • Auditory brain stem response • Auditory evoked magnetic fields • Loudness • Annoyance

2.1 Human Hearing System

The main function of hearing system is to get information about the outside, which is carried by pressure variations in the air, that is, sound wave. Sound waves are generated by the movement or vibration of an object, that is, sound source. As the vibrating object moves out and in, the nearby air molecules create a slight increase and decrease in pressure, called condensation and rarefaction, respectively. From the pressure variations, we perceive what the sound source is and where it comes from.

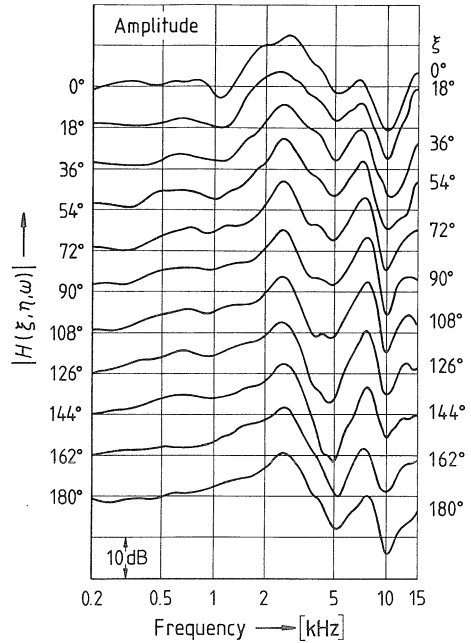
We perceive a sound wave, which is a continual time series signal, by the ears. We also perceive three-dimensional acoustic space by the ears, mainly because the head-related transfer function (HRTF) between a point of a sound source and the two ear entrances has directional characteristics from the shapes of the head and the pinnae. The pinnae significantly modify the incoming sound, particularly at high frequencies, and this is important in our ability for sound localization (Gardner and Gardner 1973; Butler and Belundiuk 1977). HRTF includes the interaural time and interaural level differences.

Figure 2.1 shows the example of amplitude of the HRTF, $H(\zeta, \eta, \omega)$, as a parameter of angle of incidence ζ (Mehrgardt and Mellert 1977). The angles ζ and η indicates azimuth and elevation angle, respectively. The angle $\zeta = 0^\circ$ corresponds to the frontal direction and $\zeta = 90^\circ$ corresponds to the lateral direction toward the side of the ear being examined.

After a sound wave arrives nearby, it passes through the peripheral auditory system, the outer ear, middle ear, and inner ear. The outer ear is the external part of the auditory system, including the pinnae and the ear canal. Sound travels down the ear canal and causes the eardrum, or tympanic membrane, to vibrate. Because of the resonance of the outer ear, we are more sensitive to sound frequencies between 1000 and 6000 Hz. The transfer function of the ear canal, $E(\omega)$, is shown in Fig. 2.2 (Wiener and Ross 1946; Shaw 1974; Mehrgardt and Mellert 1977).

The middle ear is the air-filled space between the eardrum and the cochlea that contains the ossicles. The acoustic vibrations on the eardrum are transmitted through the middle ear by three small bones, malleus, incus, and stapes, to the oval window of the cochlea. The middle ear acts as an impedance-matching device or transformer that improves sound transmission and reduces the amount of reflected sound. This is accomplished mainly by the differences in effective areas of eardrum and the oval window and to a small extent by the lever action of the ossicles. Transmission of sound through the middle ear, $C(\omega)$, is most efficient at frequencies between 500 and 4000 Hz as shown in Fig. 2.3 (Puria et al. 1997; Aibara et al. 2001).

Fig. 2.1 Transfer functions (amplitude) from a free field to the ear canal entrance as a parameters of angle of incidence ζ (Mehrgardt and Mellert 1977)



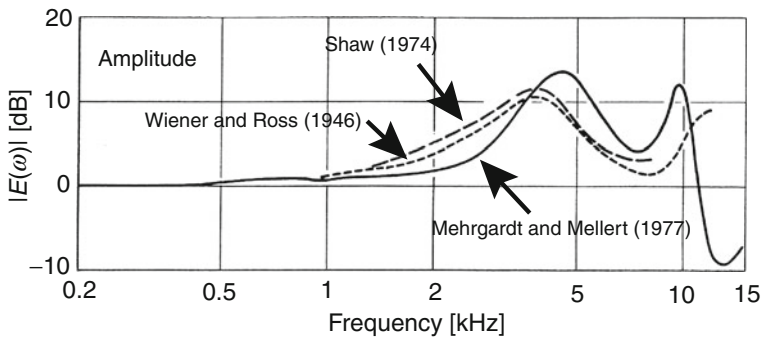
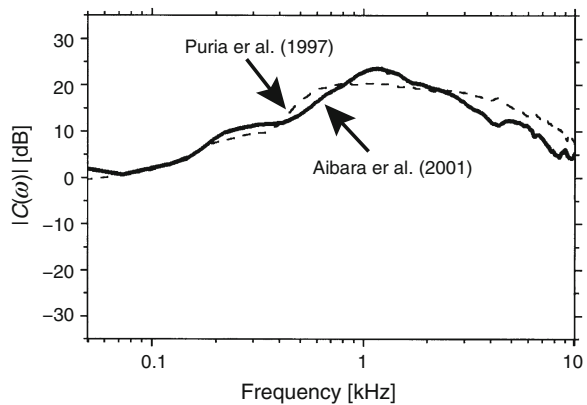


Fig. 2.2 Transfer functions (amplitude) of the ear canal (Mehrgardt and Mellert 1977)

Fig. 2.3 Transfer functions (amplitude) of the middle ear (Aibara et al. 2001)



For the usual sound field, the transfer function between a sound source located in front of the listener and the cochlea, $S(\omega)$, may be represented by

$$S(\omega) = H(\xi, \eta, \omega)E(\omega)C(\omega). \quad (2.1)$$

The values are plotted in Fig. 2.4 (Ando 1998). The pattern of the transfer function agrees with the ear sensitivity for people with normal hearing estimated from equal-loudness-level contours at 40 phon (ISO 226:2003).

The inner ear is the part of the ear that is filled with fluid, including the cochlea and semicircular canals. Sound enters the cochlea through the oval window covered by a membrane. When the oval window moves due to the pressure from the stapes, Reissner's membrane and the basilar membrane are pushed down, and the round window moves out. It follows that vibration of the stapes leads to vibration of the basilar membrane. The basilar membrane separates out the frequency components of a sound. At the base of the cochlea, near the oval window, the basilar membrane is narrow and stiff and is sensitive to high frequencies. At the apex of the cochlea,

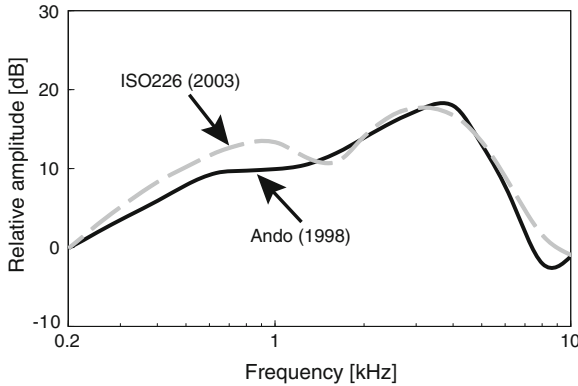


Fig. 2.4 Sensitivity of the human ear to a sound source in front of the listeners estimated from transformation characteristics between the sound source and the cochlea, $S(\omega) = H(\omega)E(\omega)C(\omega)$, (Ando 1998) and equal-loudness-level contours at 40 phon (ISO 226)

the other end of the membrane is wide and loose and is sensitive to low frequencies. The basilar membrane behaves as a band of overlapping band-pass filters, which is called auditory filters.

The mechanical vibrations of the basilar membrane are converted into electrical activity in the auditory nerve. This task is accomplished by the inner hair cells. Vibration of the basilar membrane causes a displacement of a stereochilia at the tips of the hair cells which lies within the organ of Corti on the basilar membrane, and this leads to action potentials (spikes) within the nerve fibers of the auditory nerve. Because each inner hair cell is attached to a specific place on the basilar membrane, each neuron in the auditory nerve carries information about the vibration of the basilar membrane at a single place in the cochlea. This means each neuron in the auditory nerve is sensitive to each characteristic frequency.

The auditory nerve carries the information about incoming sound from the cochlea to the cochlea nucleus. Cells of the cochlear nucleus project to higher nuclei through ventral and dorsal streams (Pickles 2008). Cells that project via a ventral stream primarily project to the superior olivary complex (SOC). The SOC is divided into three primary nuclei: the medial superior olive (MSO), lateral superior olive (LSO), and the medial nucleus of the trapezoid body (MNTB). The timing and intensities of the stimuli at the two ears are compared in the SOC, and the information is used for sound localization. Cells that project via a dorsal stream project mainly to the contralateral lateral lemniscus nuclei (LMN) and inferior colliculus (IC). They are involved in the complex analysis of a sound.

The ventral stream, mainly involved in sound localization, runs primarily to the SOC. The stream has two divisions. In the first division, the intensities of the stimuli at the two ears are compared in the LSO. In the second division, the timing of the stimuli in the two ears is compared in the MSO. The dorsal stream, mainly involved in sound identification, runs primarily to the IC of the opposite side, some fibers synapsing in the LMN on the way.

The IC is the main receiving station for the ascending pathways from lower stages of the brain stem. It forms the primary site of convergence of the sound identification and sound localization streams. It is suggested that this is a critical stage in transformation from responses dominated by the simple acoustic characteristics, to those which integrate acoustic properties in a way that begins to define an auditory object (Pickles 2008).

The medial geniculate body (MGB) is the specific thalamic auditory relay of the auditory system, receiving afferent from the IC, and projecting to the cerebral cortex. It also has heavy reciprocal connections back from the cortex, indicating that the cortex and MGB are grouped together as a functional unit.

The auditory cortex consists of core areas, surrounded by belt and parabelt areas. Previous studies suggest that the core area is necessary for the response to basic features of a sound, while the belt and parabelt areas are necessary for the response to complex features. It is suggested that the auditory cortex is necessary for the representation of auditory objects, that is, the assembly of information about all features of a sound (Pickles 2008).

To evaluate sound qualities, it is necessary to consider our auditory functioning, that is, how incoming sound is processed from the peripheral to central auditory system.

2.2 Neural Evidences of the Autocorrelation Model in the Auditory Pathways

A model for evaluations of environmental noise has been proposed based on human auditory system (Ando 2001). The model of the auditory-brain system includes the autocorrelation function (ACF) mechanism, which might exist in the auditory nerve, and the interaural cross-correlation function (IACF) mechanism, which might exist in the IC. Temporal and spatial sensations may be processed in the left and right hemisphere according to the temporal factors extracted from the ACF and the spatial factors extracted from the IACF, respectively, which is discussed in Chaps. 3 and 4. The overall subjective responses, for example, subjective preference and annoyance, may be processed in both hemispheres in relation to the temporal and spatial factors (Ando 2002).

The internal ACF may provide a representation for judging pitch salience. In temporal models of pitch perception, it is assumed that the pitch is extracted with autocorrelation (Licklider 1951; Bilsen and Ritsma 1969; Wightman 1973; Yost and Hill 1979; Meddis and Hewitt 1991; Patterson et al. 1995). Regarding the pitch salience or strength of pitch, psychophysical research has revealed that the strength of the pitch corresponds well to the peak amplitude of the ACF of the auditory signal, which represents the degree of temporal regularity of the sound (Wightman 1973; Yost et al. 1996; Yost 1996; Ando et al. 1999). One type of sound that allows for systematic manipulation of pitch salience is iterated rippled noise (IRN). IRN is produced by adding a delayed copy of a noise to the original noise and then

repeating this delay-and-add process (Bilsen 1966; Yost 1996). A normalized ACF of IRN reveals a peak at the reciprocal of the delay, whose magnitude grows with increasing number of iterations reflecting the increasing periodicity.

Physiologically, recordings of responses to IRN stimuli from auditory nerve fibers (Fay et al. 1983; ten Kate and van Bekkum 1988) and cochlear nucleus neurons (Bilsen et al. 1975; Shofner 1991, 1999; Winter et al. 2001) show that the pitch of IRN is represented in the firing patterns of action potentials locked to either the temporal fine structure or envelope periodicity. That is, there is temporal regularity in the fine structure of the neural firing patterns, and it produces peaks in the autocorrelogram. These data suggest that the pitch of IRN stimuli is based on ACF mechanism. Indeed, the pooled interspike interval distributions of auditory nerve discharge patterns in response to complex sounds resemble the ACF of the stimulus waveform, and the magnitude of the ACF peak corresponds well with pitch salience (Cariani and Delgutte 1996a, b).

Electroencephalography (EEG), the measurement of electric potential differences on the scalp, is a widely applied method for investigating the functions of the human brain. Magnetoencephalography (MEG) is closely related to EEG. In both methods, the measured signals are generated by the same synchronized neuronal activity in the brain. The time resolution of EEG and MEG is in the millisecond range. Thus with EEG and MEG, it is possible to follow the rapid changes in cortical activity that reflect ongoing signal processing in the brain; the electrical events of single neurons typically last from one to several tens of milliseconds (Hämäläinen et al. 1993).

Several types of stimulus-evoked brain stem neural activity may be recorded using the EEG. Best known and most extensively studied EEG is the auditor brain stem response (ABR). Another type of brain stem neural activity is the frequency-following response (FFR). Unlike the ABR, the FFR reflects sustained neural activity (integrated over a population of neural elements) that is phase-locked to the individual cycles of the stimulus waveform and/or the envelope of periodic stimuli (Krishnan 2007).

The ABR and auditory evoked magnetic field (AEF) were recorded and analyzed to identify such ACF mechanism in human brain. FFRs were recorded from seven listeners in response to IRNs, which varied only in their degree of pitch salience (Krishnan et al. 2010). The FFR reflects sustained phase-locked activity in a population of neural elements within the rostral brain stem (e.g., Krishnan 2007; Chandrasekaran and Kraus 2010).

To create IRN stimuli with a dynamic fundamental frequency (F_0) contour whose pitch varies as a function of time, a time-varying delay-and-add algorithm to a filtered Gaussian noise (10–3000 Hz) was applied (Denham 2005). The pitch increases in a curvilinear fashion from about 100 to 135 Hz over the 250-ms stimulus duration. By using a different number of iterations (n) in the IRN generating circuit, the F_0 contour's pitch salience was varied. FFRs were recorded from each listener in response to monaural stimulation of the right ear at 80 dB sound pressure level (SPL) through a magnetically shielded insert earphone (Etymotic, ER-3A) (Krishnan et al. 2010). Neural responses were recorded differentially

between a noninverting (+) electrode placed on the midline of the forehead at the hairline (Fz) and inverting electrodes (−) placed on the left (A1) and right (A2) mastoid, and the 7th cervical vertebra (C7). Another electrode placed on the mid-forehead (Fpz) served as the common ground. FFRs were recorded simultaneously from the three different electrode configurations and subsequently averaged for each stimulus condition to yield a response with a higher signal-to-noise ratio.

To analyze the robustness of encoding to stimuli differing in pitch salience, the neural pitch strength of each response waveform was quantified. From each FFR, the normalized ACF calculated over the entire duration of the response was computed in order to determine the dominant periodicities contained within the response. The height of the first peak in the ACF from time-delay zero was taken as the magnitude of neural pitch strength (Krishnan et al. 2005). In all cases, this peak fell at a delay of 10 ms, the fundamental pitch period of the input stimulus (Fig. 2.5). The growth in FFR pitch strength (derived from peak magnitude of the FFR ACF) with increasing iteration steps suggests an increase in the degree of neural phase-locking to the pitch relevant periodicity resulting from increased temporal regularity in the stimulus.

In addition, behavioral frequency difference limens (F0 DLs) were measured from each listener to obtain a perceptual estimate related to pitch salience. F0 DLs decreased with increasing stimulus periodicity revealing better pitch change detection for more salient stimuli. The strong correlation observed between the neural and behavioral measures supports the view that ACF-related pitch encoding at a subcortical and sensory level of processing plays an important role in shaping pitch perception.

MEG has been used to investigate how features of sound stimuli related to pitch are represented in the human auditory cortex. Focused on a spatial representation of pure tone in the auditory system according to their frequency, tonotopic organization of the human auditory cortex has been investigated (e.g., Elberling et al. 1982; Romani et al. 1982; Pantev et al. 1988, 1995). Focusing on the temporal structure of the sound, the periodicity pitch-related cortical response has been investigated (Pantev et al. 1989; Langner et al. 1997; Cansino et al. 2003; Fujioka et al. 2003; Seither-Preisler et al. 2003).

AEFs in relation to bandwidth variations of band-pass noise have been examined (Soeta et al. 2005a, 2006). The results indicate that the peak amplitude of N1m, which is found above the left and right temporal lobes around 100 ms after the stimulus onset, decreases with increasing bandwidth of the band-pass noise. The peak amplitude of the ACF increases with decreasing bandwidth of the auditory stimuli (Merthayasa et al. 1994; Sato et al. 2002; Soeta et al. 2004a). The pitch strength of band-pass noises was found to increase with decreasing bandwidth (Fastl and Stoll 1979). Therefore, it was assumed that sounds that have larger peak amplitude of the ACF or stronger pitch could lead to more cortical activity, which would cause an increase in the strength of the N1m response.

To evaluate responses related to pitch salience, which is characterized by the peak amplitude of the ACF of the sound, in auditory cortex, the AEFs elicited by

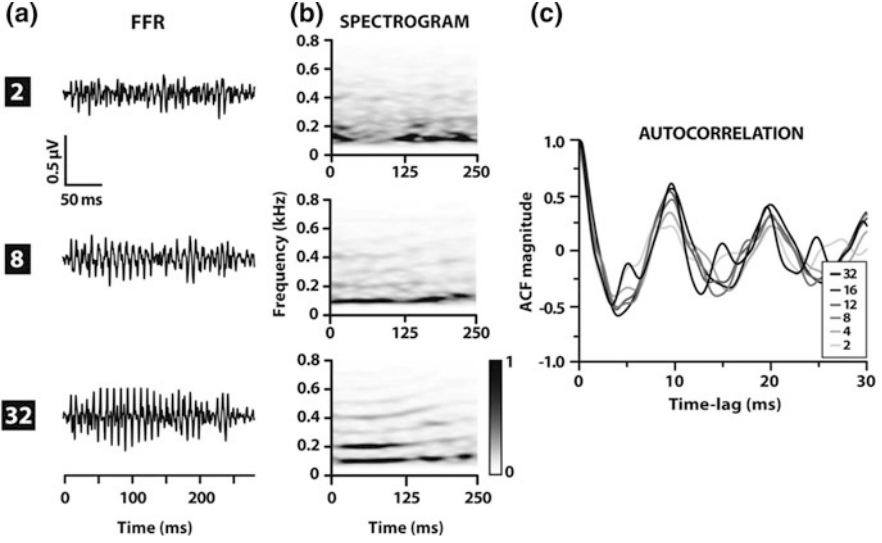


Fig. 2.5 FFR waveforms (a), spectrograms (b), and ACFs (c) as a function of iteration steps (n) computed from grand averaged brain stem responses. Spectrograms were computed by sliding a 50-ms analysis window by a 1 ms increment and computing the FFT in each time bin. Normalized magnitudes are indicated by the *gray-scale* gradient; *darker shades* indicate stronger encoding of pitch relevant harmonics (i.e., more pronounced phase-locked activity). Minimal periodicity is observed in FFRs at low iteration steps ($n = 2$; *top row*). By $n = 8$ iterations, FFR phase-locked activity captures periodicity related to the fundamental frequency (F_0) and its harmonics (*middle row*). Robust encoding is even more pronounced at $n = 32$ iterations when the stimulus is maximally salient (*bottom row*). Temporal waveforms and ACFs derived from the FFRs reveal increasing periodicity in the neural response with increasing iteration steps, thus indicating more robust brain stem activity for salient pitch (Krishnan et al. 2010)

IRN with different iteration numbers were recorded (Soeta et al. 2005b). It was anticipated that the N1m amplitude would increase with an increase in the number of iterations of the IRN.

Ten normal hearing listeners (22–31 years, all right-handed) took part in the experiment. The IRN was produced by a delay-and-add algorithm applied to band-pass noise that was filtered using fourth-order Butterworth filters between 400 and 2200 Hz. The number of iterations of the delay-and-add process was set at 0, 1, 4, and 16. The delay was fixed at 1 ms, corresponding to a pitch of 1000 Hz. The stimulus duration used the experiment was 0.5 s, including rise and fall ramps of 10 ms. The auditory stimuli were delivered to the listeners through plastic tubes and inserted earpieces at a comfortable listening level adjusted separately for each listener. Figure 2.6 shows the temporal waveforms and the power spectra of some of the stimuli measured with an ear simulator that includes a microphone, a pre-amplifier, and an adaptor connected to the earpiece. Figure 2.7 shows the ACF of some of the stimuli measured with the ear simulator. The τ_1 of IRN corresponds to the delay. The ϕ_1 increases as the number of iterations increases.

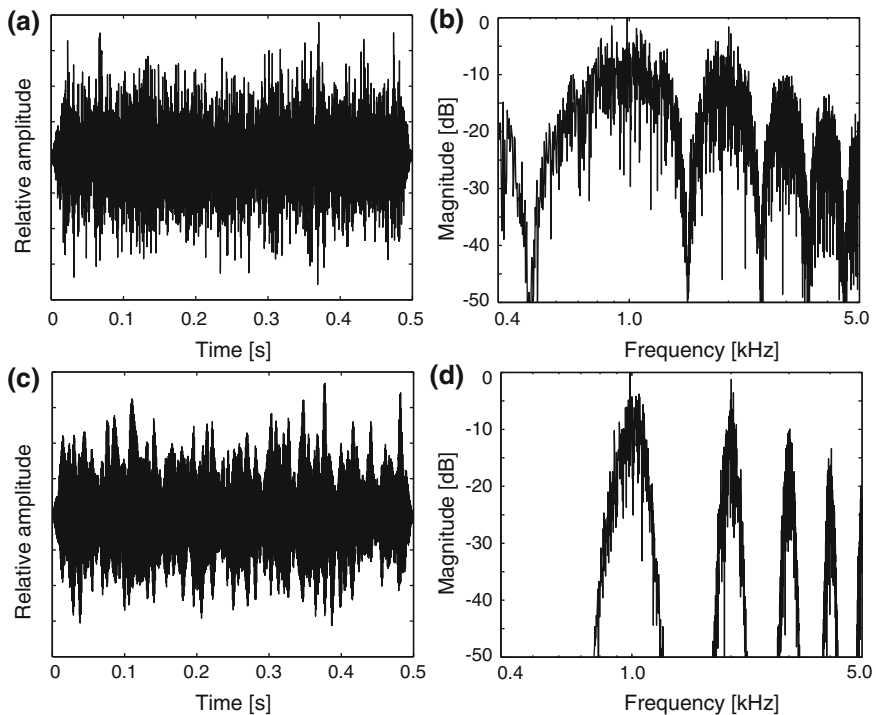
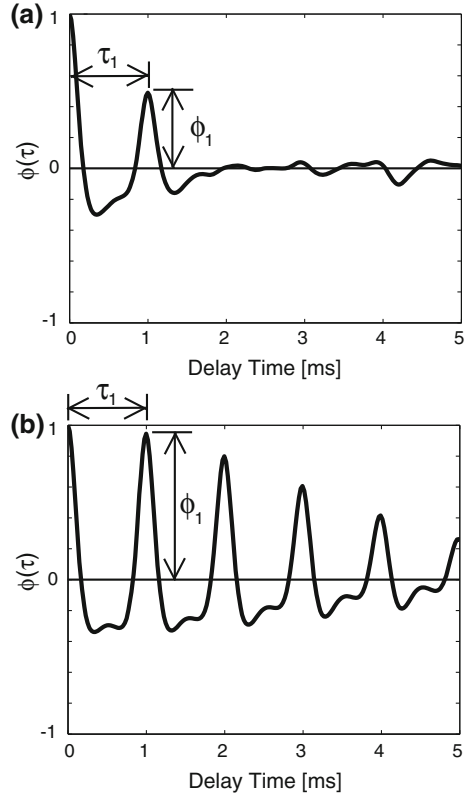


Fig. 2.6 Temporal waveforms and power spectra of the IRN with the number of the iterations (a, b) 1 and (c, d) 16 (Soeta et al. 2005b)

The AEFs were recorded using a 122 channel whole-head DC superconducting quantum interference device (DC-SQUID) magnetometer (Neuromag-122TM, Neuromag Ltd., Helsinki, Finland) in a magnetically shielded room (Hämäläinen et al. 1993). The IRNs were presented in randomized order with a constant inter-stimulus interval of 1.5 s. Listeners were instructed to watch a self-selected silent movie and to ignore the stimuli. The magnetic data were sampled at 0.4 kHz after being band-pass filtered between 0.03 and 100 Hz and then averaged approximately 50 times. The averaged responses were digitally filtered between 1.0 and 30.0 Hz. The analysis time was 0.7 s from 0.2 s prior to the stimulus onset, with an average prestimulus period of 0.2 s serving as the baseline. The Neuromag-122TM has two pick-up coils in each position that measure two tangential derivatives, $\partial B_z/\partial x$ and $\partial B_z/\partial y$, of the field component B_z . With such a coil configuration, the largest signal occurs just above a dipolar source where the gradient is steepest (Knuutila et al. 1993). To evaluate the amplitude and latency of the N1m peak, the root-mean-squares (RMS) of $\partial B_z/\partial x$ and $\partial B_z/\partial y$ were determined as the amplitude of the responses at each recording position. The N1m peak amplitude and latency were defined as the RMS peak and latency in the latency range from 70 to 130 ms over

Fig. 2.7 ACFs of the IRN with the number of the iterations **a** 1 and **b** 16 (Soeta et al. 2005b)



the right and left hemispheres. In each listener, we employed the N1m peak latency and amplitude with a channel that showed the maximum amplitude placed at each hemisphere.

To estimate the location and strength of the underlying neural activity of the N1m wave, a single equivalent current dipole (ECD) was assumed as the source of the magnetic field of the N1m wave in a head-based coordinate system. The ECDs that best described the measured magnetic field at the N1m peak latencies were found by least squares fitting in a spherical volume conductor (Kaukoranta et al. 1986). A one-dipole model was used separately for the left and right hemispheres, with a subset of channels over each hemisphere. The origin of this coordinate system was set at the midpoint of the medio-lateral axis (y-axis) which joined the center points of the entrance to the acoustic meatuses of the left and right ears. The posterior–anterior axis (x-axis) was oriented from the origin to the nasion, while the inferior–superior axis (z-axis) was perpendicular to the x–y plane. All ECDs with goodness-of-fit values exceeding 80 % were used in further analyses.

Clear N1m responses were observed in both the right and left temporal regions in all listeners (Fig. 2.8). The N1m latencies were not systematically affected by the number of iterations of the IRN. Figure 2.9 depicts the mean N1m amplitude

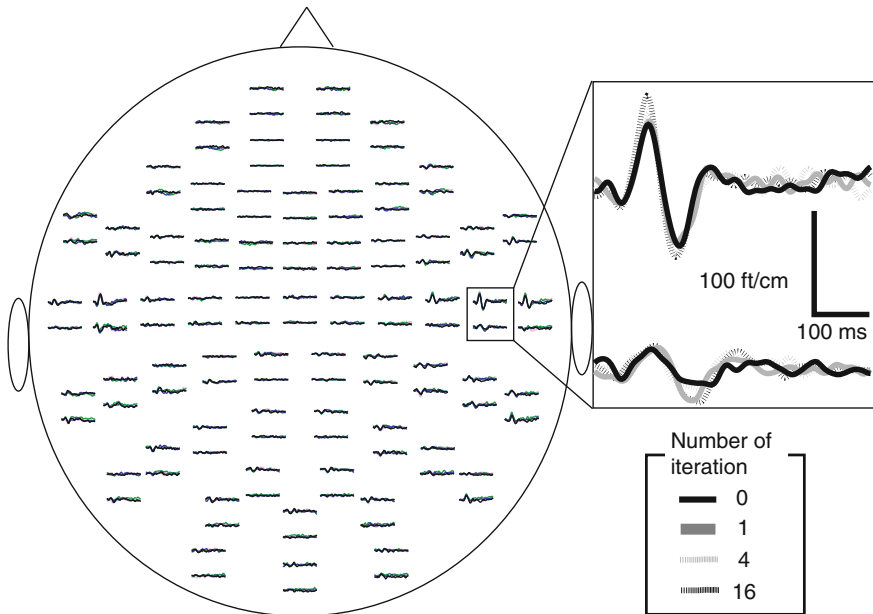


Fig. 2.8 Typical waveforms of auditory evoked magnetic fields from 122 channels in a listener (Soeta et al. 2005b)

(across ten listeners) as a function of the number of iterations. A greater number of iterations of the IRN produced a larger N1m amplitude, that is larger ϕ_1 of the stimulus produced a larger N1m response. A two-way analysis of variance (ANOVA) (number of iterations \times hemisphere) revealed a significant main effect of the number of iterations on the N1m peak amplitude. This result is consistent with the previous study using band-pass noise with variation of bandwidth (Soeta et al. 2005a, 2006) and IRN with a delay of 2, 4, or 16 ms (Krumbholz et al. 2003; Soeta and Nakagawa 2008a). The amplitude of the AEF component in response to periodic stimuli was compared with simulated peripheral activity patterns of the auditory nerve (Seither-Preisler et al. 2003). The results showed that the amplitude of the N1m is correlated with the pitch strength estimated on the basis of auditory nerve activity. This result is consistent with the present results.

For the dipole strength, similar results to those for the N1m peak amplitude were obtained. A greater number of iterations of IRN produced a larger N1m ECD moment. A two-way ANOVA revealed a significant main effect of the number of iterations of IRN on the ECD moments. The ECD locations did not show any systematic variation across the listeners as a function of the number of iterations of IRN.

Figure 2.10 shows the relationship between ϕ_1 of the stimulus and ECD moment of the N1m response. To compare the previous result, the results of band-pass noise with center frequency of 1000 Hz were also included in Fig. 2.10 (Soeta et al. 2006). Psychophysical studies have indicated that first peak of the ACF, ϕ_1 , could

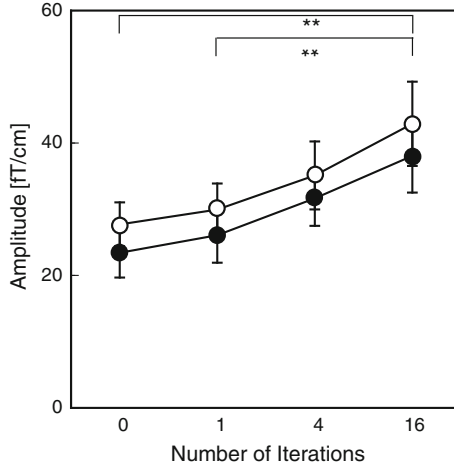


Fig. 2.9 Mean amplitude of the N1m (\pm SEMs) as a function of the number of iterations from the right (*filled circle*) and left (*open circle*) hemispheres. The *asterisks* indicate statistical significance ($*P < 0.05$, $**P < 0.01$; Post hoc Bonferroni test) (Soeta et al. 2005b)

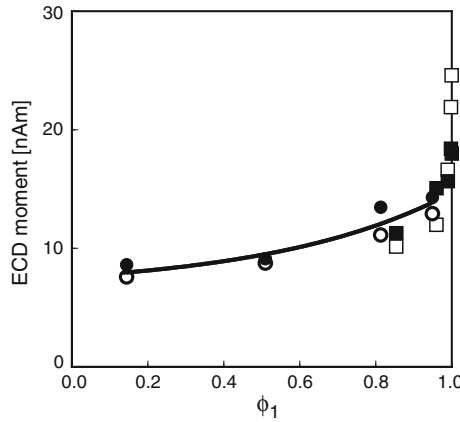


Fig. 2.10 Relationship between peak amplitude of the ACF, ϕ_1 , and ECD moment of the N1m from the right (*filled circle*) and left (*open circle*) hemispheres. The curve is of the form $6.6 + 100.9\phi_1$ (Soeta et al. 2005b). The previous ECD moment of the N1m in response to band-pass noise with center frequency of 1000 Hz from the right (*filled square*) and left (*open square*) hemispheres were also included for comparison (Soeta et al. 2006)

account for the pitch strength of the stimulus (Wightman 1973; Yost et al. 1996; Ando et al. 1999) and pitch strength of IRN was an exponential function of ϕ_1 , namely of the form $a + 10b\phi_1$, where “ a ” and “ b ” are constants (Yost 1996). Note that, the ECD moment derived in the current study could also be described in the form $a + 10b\phi_1$, where $a = 6.6$ and $b = 0.9$, as shown in Fig. 2.10.

The pitch onset response (POR) was introduced to circumvent the energy onset response (EOR), such as N1m, and thereby isolate the response of those neural elements specifically in pitch processing (Krumbholz et al. 2003). The POR is a negative component of the AEF, which can be elicited by the transition from a noise to a tone even when there is no concurrent change in sound energy. The results showed that the amplitude of the POR is correlated with the pitch strength, that is to say, the number of iterations of the IRN, suggesting that the underlying generators are part of a pitch-processing network. This is consistent with N1m results (Soeta et al. 2005b; Soeta and Nakagawa 2008a). The results also show that the source of the POR lies somewhat anterior and inferior to that of the N1m. Then, whether the POR originates from the same generator as the EOR was examined (Seither-Preisler et al. 2004). The results suggest an interaction between the POR and the EOR, which may be based on common generators. Given this, the N1m responses derived in our study (Soeta et al. 2005b; Soeta and Nakagawa 2008a) are considered to include both the EOR and POR responses. However, the stimulus used in the study had the same SPL and the same stimulus onset. Consequently, the effect of the number of iterations of the IRN on N1m is contributed mainly by a pitch-processing network.

2.3 Neural Evidences of the Interaural Cross-Correlation Model in the Auditory Pathways

The internal binaural IACF may provide a representation for judging subjective preference and spatial sensations. The psychological responses to IACF factors have largely been obtained in humans, while the neurophysiological responses are confined to animal studies (Yin et al. 1987; Saberi et al. 1998; Palmer et al. 1999). The ABR and AEF were recorded and analyzed to identify such a mechanism in human brain.

To probe the neural correlates of horizontal sound direction (azimuth), the source signals $p(t)$ of trains of clicks (50- μ s pulses) were presented every 100 ms for 200 s (2000 times) and the left and right ABRs were recorded through electrodes placed on the vertex and the left and right mastoids (Ando and Hosaka 1983; Ando 1985). Signals were supplied to loudspeakers positioned at various horizontal angles (0°–180°) with respect to the front of the listener, all on the listener's right-hand side. The distance between each loudspeaker and the center of the head was kept at 68 ± 1 cm. The speakers had a frequency response of ± 3 dB for 100 Hz–10 kHz.

Typical examples of recorded ABR waveforms as a function of the horizontal angle of sound incidence are shown in Fig. 2.11. It can be appreciated that waves I–VI differ in peak amplitude and latency as the sound location changes its angle of incidence relative to the listener's head. Similar ABR waveforms were obtained from each of four listeners (males, 23 ± 2 years of age). Their ABRs were averaged together, and the mean amplitude of the ABR waveform peaks (waves I–VI) was computed as a function of the horizontal angle (Fig. 2.12a–f). Of particular interest is

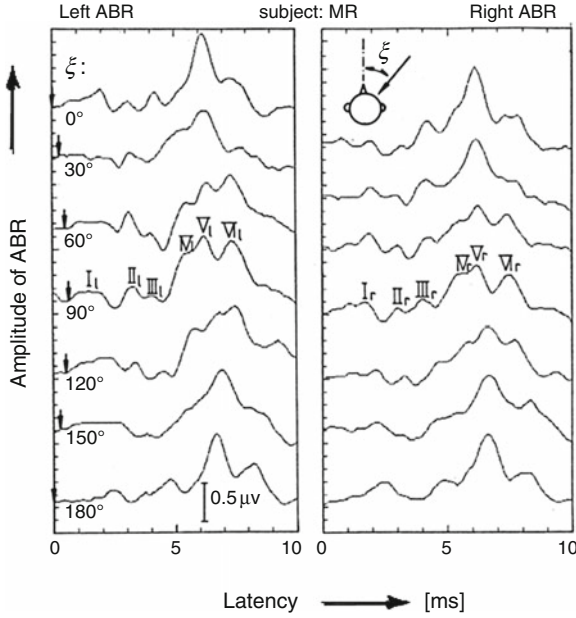


Fig. 2.11 Examples of ABR obtained between the vertex and left and right mastoids as a function of the latency less than 10 ms and a parameter of *horizontal* angle of sound incidence. The abscissa is the latency in the auditory pathways relative to the time when the single pulse arrives at the right ear entrance. *Arrows* indicate the time delay, which depends upon the sound source location on the right-hand side of the listener, and the null amplitude of ABR. The wave number is defined by the symbol from $I_{l,r}$ to $VI_{l,r}$, which is reflected by the activity at each nucleus (relay station) in the auditory systems. The suffix signifies the left and right auditory pathway (Ando et al. 1991)

that the average peak I amplitudes from the right electrode are greater than those from the left, $r > l$ for angles $\xi = 30^\circ\text{--}120^\circ$ ($p < 0.01$), which may reflect interaural differences in sound pressure (head shadowing) produced by the source location on the right-hand side. This tendency is reversed for wave II for two angles $\xi = 60^\circ\text{--}90^\circ$ ($l > r, p < 0.05$; Fig. 2.12b). The behavior of wave III (Fig. 2.12c) is similar to that of wave I ($r > l, p < 0.01$). This tendency again reverses for wave IV ($l > r, p < 0.05$; Fig. 2.12d) and is maintained further in wave VI ($l > r, p < 0.05$; Fig. 2.12f) even though absolute values are amplified.

From these patterns, it could be inferred that the flow of the left and right neural signals is interchanged 3 times at the cochlear nucleus, the SOC, and the LLN as shown in Fig. 2.13. The interaction at the IC in particular may be operative for the interaural signal processing as discussed later. In wave V as shown in Fig. 2.12e, such a reversal cannot be seen, and the relative behavior of amplitudes of the left and the right is parallel and similar. Thus, these two amplitudes were averaged and plotted in Fig. 2.14 (V symbols). For comparison, the amplitudes of wave IV [left (l) and right (r)] normalized to their respective ABR amplitudes at the frontal sound

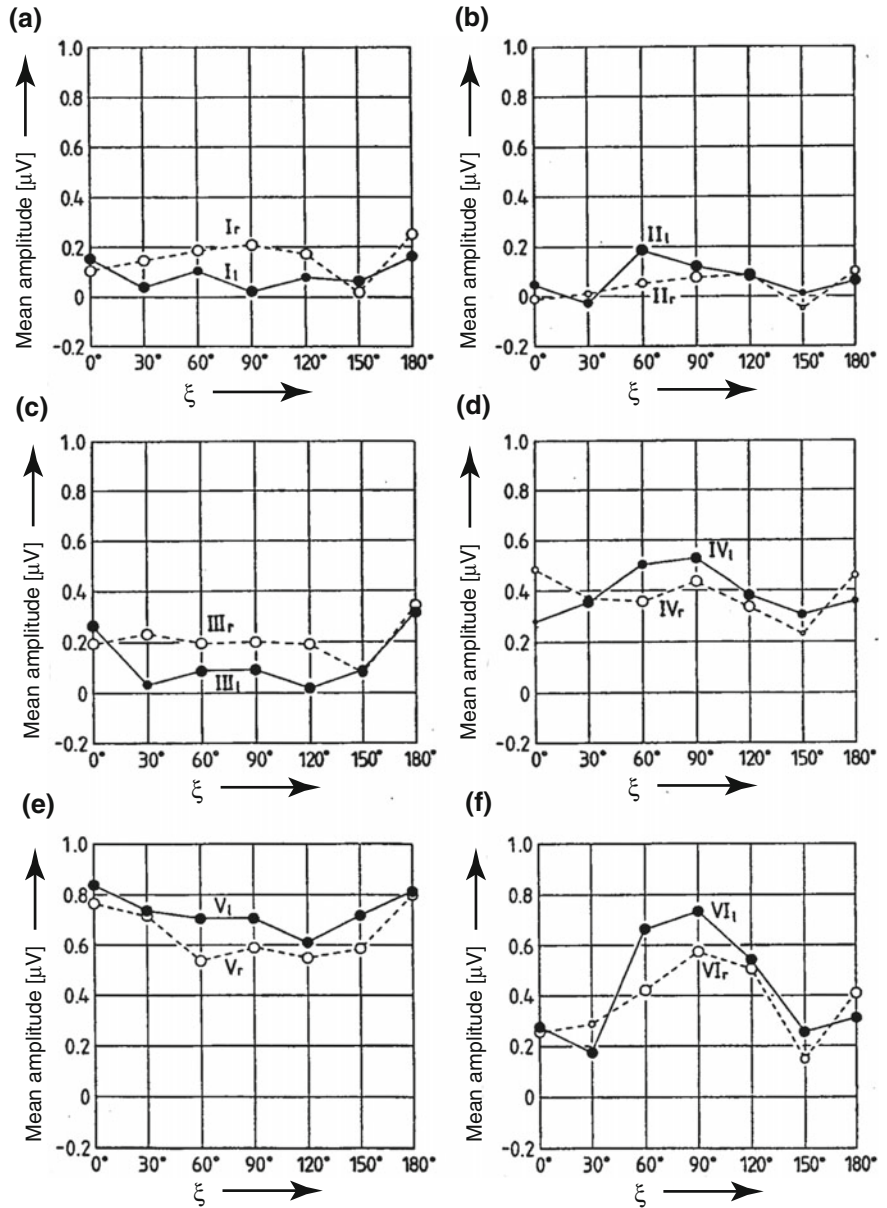


Fig. 2.12 Averaged amplitudes of ABR for each wave I-VI. The size of *circles* indicated the number of available data from four listeners. *Filled circles* left ABRs; *open circles* right ABRs. **a** Wave I. **b** Wave II. **c** Wave III. **d** Wave IV. **e** Wave V. **f** Wave VI (Ando et al. 1991)

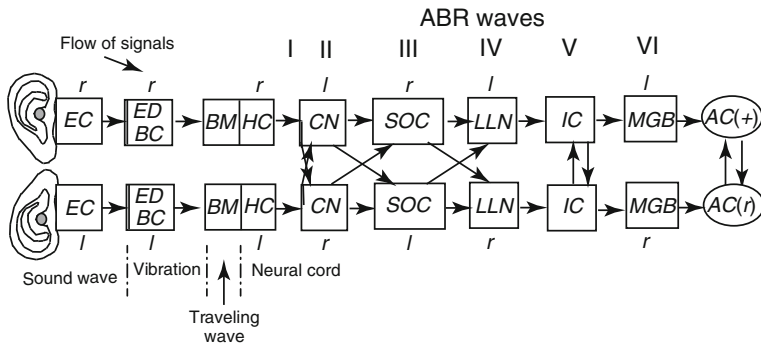


Fig. 2.13 Schematic illustration of the flow of neural signals in auditory pathways. *EC* external canal; *ED* and *BC* eardrum and bone chain; *BM* and *HC* basilar membrane and hair cell; *CN* cochlear nucleus; *SOC* superior olivary complex; *LLN* lateral lemniscus nucleus; *IC* inferior colliculus; *MGB* medial geniculate body; and *AC* auditory cortex of the right and left hemispheres

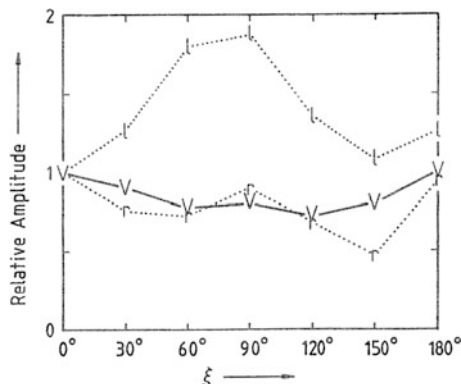


Fig. 2.14 Averaged amplitudes of ABR waves IV_l (symbol: l) and IV_r (symbol: r), and averaged amplitudes of waves V_l and V_r (symbol: V) normalized to the amplitudes at the frontal incidence (four listeners) (Ando et al. 1991)

incidence, which may correspond to the normalized sound pressures at the right and left ear entrances, respectively, are also plotted.

Neural ABR responses can be compared with cross-correlations derived from acoustical measurements at the two ears of a dummy head. A-weighted signals were presented and free-field sound pressure measurements were taken at the two ear entrances of a dummy head as a function of the horizontal angle of the sound source. Figure 2.15 depicts the signal power at the two ears (R, L) for different angles (the zero-lag term of the ACFs) and the maximum value of the IACF (ϕ), which are normalized only by the respective values at $\xi = 0^\circ$. Received signal power is the greatest for the ear ipsilateral to the speaker R when it is situated 90° and least for the contralateral ear. These acoustic measures can be compared with

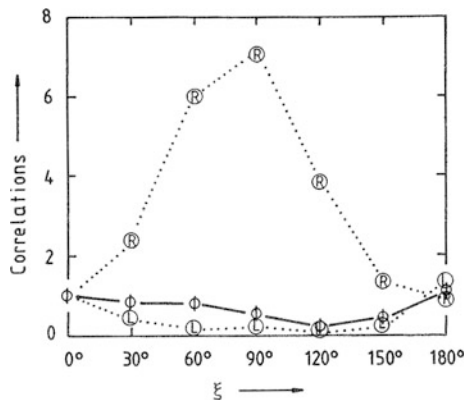


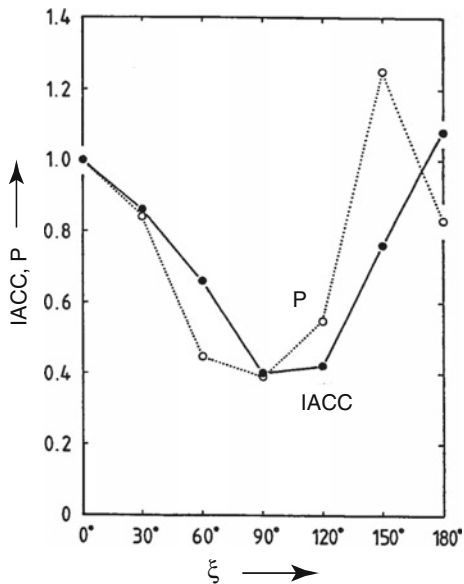
Fig. 2.15 Correlations of sound signals arriving at the left and right ear entrances of a dummy head, which are normalized by the respective values at $\xi = 0^\circ$. L $\Phi_{ll}(0)$ measured at the left ear; R $\Phi_{rr}(0)$ measured at the right ear; Φ : maximum interaural cross-correlation, $|\Phi_{lr}(\tau)|_{\max}$, $|\tau| < 1$ ms (Ando et al. 1991)

the neurally generated ABR potentials (see Fig. 2.14). Here, the neural correlate of the relative power of the received signals at the left and right ears is the average of the peak amplitudes of waves IV and V (left and right), normalized to those at the frontal incidence ($\xi = 0^\circ$). Similar results are obtained when amplitudes are normalized to those at $\xi = 180^\circ$. Although differences in units and scaling confound direct comparison between the results in Figs. 2.14 and 2.15, there are nevertheless qualitative similarities between these acoustic and physiologic responses. The relative behavior of wave IV (l) in Fig. 2.14 is similar to $\Phi_{rr}(0)$ in Fig. 2.15, which was measured at the right ear entrance r . Also, the relative behavior of wave IV r is similar to $\Phi_{ll}(0)$ at the left ear entrance l . In fact, amplitudes of wave IV (left and right) are proportional to $\Phi_{rr}(0)$ and $\Phi_{ll}(0)$, respectively, due to the interchange of signal flow. The behavior of wave V is similar to that of the maximum value, $|\Phi_{lr}(\tau)|_{\max}$, $|\tau| < 1$ ms. Because correlations have the dimensions of the power of the sound signals (i.e., the square of ABR amplitude), the interaural cross-correlation coefficient (IACC), which is defined by the maximum value of the IACF, may correspond to

$$P = \frac{A_V^2}{A_{IV,r}A_{IV,l}} \quad (2.2)$$

where A_V is the amplitude of the wave V, which may be reflected by the “maximum” synchronized neural activity ($\approx |\Phi_{lr}(\tau)|_{\max}$) in the inputs to the IC (see Fig. 2.13). $A_{IV,r}$ and $A_{IV,l}$ are amplitudes of wave IV from the right and left, respectively. The results obtained by Eq. (2.2) are plotted in Fig. 2.16. It is clear that the behavior of the IACC and P are in good agreement ($r = 0.92$, $p < 0.01$).

Fig. 2.16 Values of the IACC and values of P obtained by Eq. (2.1). A linear relationship between the IACC and the P value is obtained. Note that the available data at $\xi = 150^\circ$ was a single listener (Ando et al. 1991)



The amplitudes of the ABRs clearly differ according to the horizontal angle of the incidence of sound relative to the listener (Fig. 2.12). In particular, it is found that the amplitudes of waves I_{Vl} and I_{Vr} are nearly proportional to the SPLs at the right and left ear entrances, respectively, when the amplitude is normalized to that in front or back ($\xi = 180^\circ$).

Since neurophysiological responses to IACC has examined in the auditory brain stem (Ando et al. 1991), there is little evidence of the cortical responses to IACC. To obtain such response, the present study used MEG to examine whether or not there is an activity in the auditory cortex corresponding to the IACC variations of band-pass noise.

Band-pass noises were employed for acoustic signals. To create band-pass noises, white noises were digitally filtered between 200 and 3000 Hz (Chebychev band-pass: order 18). The IACC of the stimuli was controlled by mixing in-phase diotic band-pass and dichotic independent band-pass noises in appropriate ratios (Blauert 1996). The frequency range of these noises was always kept the same. Figure 2.17 shows examples of the power spectrum, the temporal waveform, and the IACF of the stimulus used in this study. The interaural level difference was set to 0 dB, and there was no interaural delay between ear signals, i.e., the maximum of the IACC was always at $\tau = 0$.

Nine listeners with normal hearing (22–28 years, all right-handed) took part in the experiment. The AEFs were recorded using a 122 channel whole-head DC-SQUID magnetometer (Neuromag-122TM; Neuromag Ltd., Helsinki, Finland) in a magnetically shielded room (Hämäläinen et al. 1993). Combinations of a reference stimulus (IACC = 1.0) and test stimuli (IACC = 0.85, 0.6, 0.2) were presented alternately at a constant 0.5-s interstimulus interval. During the experiment, listeners

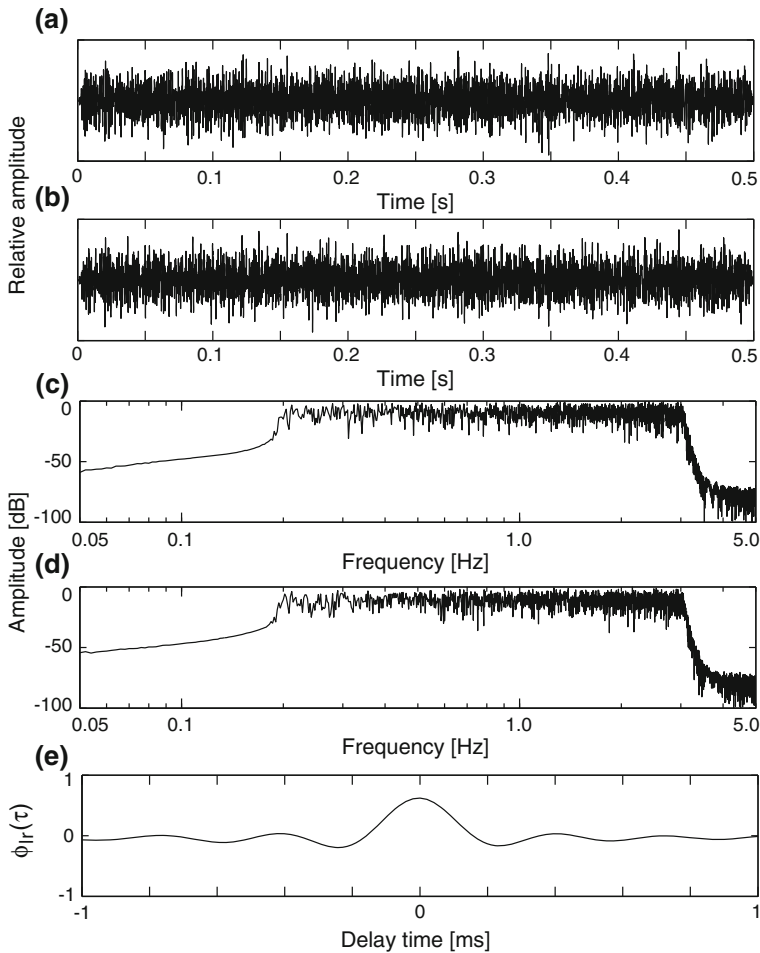


Fig. 2.17 Examples of the temporal waveform at the left (a) and right (b) ears, the power spectrum at the left (c) and right (d) ears, and the IACF (e) of the stimulus (IACC = 0.6) (Soeta et al. 2004b)

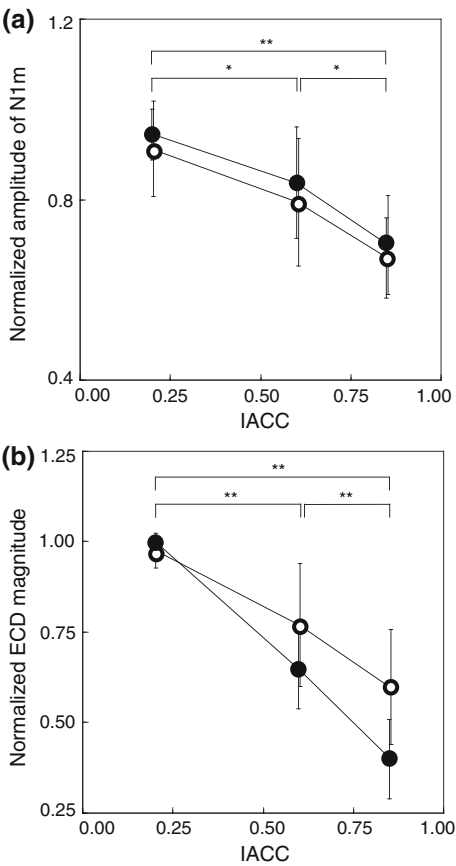
were asked to close their eyes to fully concentrate on the stimuli. The magnetic data were sampled at 0.4 kHz after being band-pass filtered between 0.03 and 100 Hz and averaged more than 50 times. Any responses coinciding with magnetic signals exceeding 3000 fT/cm were rejected from further analysis. The averaged responses were digitally filtered between 1.0 and 30.0 Hz. The analysis time was 0.7 s from 0.2 s prior to the stimulus onset. The average of the 0.2-s prestimulus period served as the baseline. To evaluate the amplitude and the latency of the response, the RMS of $\partial B_z / \partial x$ and $\partial B_z / \partial y$ were determined as the amplitude of the responses at each recording position. The N1m peak amplitude and latency were defined as the RMS peak and the latency in the latency range from 70 to 130 ms over the right and left

hemisphere. In each listener, we employed the N1m peak latency and amplitude with a channel that showed the maximum amplitude placed at each hemisphere.

To estimate the location and the strength of the underlying neural activity of the N1m wave, a single ECD was assumed as the source of the magnetic field of the N1m wave. ECDs were found by a least square search in each hemisphere at the N1m peak latencies. Calculations were based on the spherical conductor model, which takes into account the volume current within a sphere (Kaukoranta et al. 1986). All ECDs with goodness-of-fit values exceeding 80 % were used in further analyses.

Clear N1m responses were observed in both right and left temporal regions in all listeners. The N1m latencies were not systematically affected by the IACC. Figure 2.18 depicts the mean N1m amplitude (across nine listeners) as a function of the IACC. The N1m amplitudes were normalized within each listener with respect to the maximum value. Basically, a smaller IACC provided a larger N1m

Fig. 2.18 The mean amplitude (a) and the mean ECD moments (b) of the N1m from right (filled circle) and left (open circle) hemispheres as a function of IACC. Error bars are the 95 % confidence interval. The N1m amplitudes and ECD moments are normalized within each listener with respect to the maximum value. The asterisks indicate statistical significance (* $P < 0.05$, ** $P < 0.01$; Bonferroni test) (Soeta et al. 2004b)



amplitude. Two-way ANOVA ($IACC \times \text{hemisphere}$) revealed a significant effect of the IACC on N1m amplitude ($P < 0.001$). Variability in the left and right hemispheres was not significantly different. The N1m ECD moment showed similar tendency with the N1m amplitude.

A previous study on auditory evoked potential (AEP) investigated the IACC using a one-third octave band-pass-filtered noise with the center frequency of 500 Hz as a sound signal (Ando et al. 1987). The results there showed that the peak-to-peak amplitude N1–P2 decreases with increasing IACC. In the present MEG study, a higher IACC provided for a significantly smaller amplitude of N1m, P2m, and the peak-to-peak amplitude N1m–P2m (Soeta et al. 2004b). A previous study on N1m response to dichotic tones of different frequencies found that N1m increased with the interaural frequency disparity (Yvert et al. 1998). Significantly, smaller AEPs or AEFs amplitudes were obtained with binaural stimulation, compared to those obtained with monaural contralateral stimulation, indicating some kind of interference between ipsilateral and contralateral pathways (“binaural interaction”) (Pantev et al. 1986; McPherson and Starr 1993). It is considered that the more sounds differed arriving at both ears, the larger the N1m amplitude might be.

Blauert and Lindemann (1986) investigated the broadening and splitting of auditory events in dichotic listening condition with various degrees of the IACC by using a psychoacoustical mapping method. The response task of the listeners was to map the simple or multiple auditory events that they perceived during the presentation of each signal. The number of partial auditory events decreased with increasing IACC. This could result in larger magnetic field responses with a less interaurally coherent sound.

A starting point for modeling efforts in binaural hearing is the model of Jeffress (1948), which produces estimates of cross-correlation functions of its two inputs. Several theories regarding binaural systems rely on a cross-correlator to act as a comparator element for signals arriving at both the left and right ears (Colburn 1977; Lindemann 1986; Osman 1971; Osman et al. 1975; Blauert 1996). It has been shown that the central binaural neurons perform an operation very similar to the cross-correlation of the inputs (Ando et al. 1991; Palmer et al. 1999; Saberi et al. 1998; Yin et al. 1987). These inputs are transformed from the actual acoustic signal by the peripheral auditory system; and these transformations are reflected in the properties of the cross-correlations. Among various approaches to incorporating the evaluation of two interaural cues, namely interaural level difference (ILD) and interaural time difference (ITD or τ_{IACC}), into one consolidated model; a binaural cross-correlation model by contralateral inhibition was proposed (Lindemann 1986). A model using an IACF analysis of the ear input signals should be able to filter out the components of the ear input signals that are interaurally coherent (Lindemann 1986; Blauert 1996). Therefore, sounds that are interaurally more coherent could lead to more binaural inhibition, which causes the decrease of the strength of the N1m response.

To evaluate the effects of ITDs in relation to IACCs in human auditory cortex, the AEFs elicited by noises with different ITDs and IACCs were recorded and analyzed. The most important cues for sound localization in human are the

differences in ITD and ILD of the sound waves received at the two ears. ITDs can be measured by the IACF between two sound signals received at both the left and right ears, that is, τ_{IACC} . The psychological responses to ITDs in relation to IACCs have been obtained in humans (Jeffress et al. 1962; Zimmer and Macaluso 2005), and the neurophysiological responses have been limited to animal studies (e.g., Yin et al. 1987; Yin and Chan 1990; Albeck and Konishi 1995; Keller and Takahashi 1996; Saberi et al. 1998; D'Angelo et al. 2003; Shackleton et al. 2005).

IACC was controlled by the same method with the previous research (Soeta et al. 2004b). The stimulus duration used in the experiment was 0.5 s, including rise and fall ramps of 10 ms, which were cut out of a 10-s long band-pass filtered noise with varying IACC and ITD. For stimulus lateralization, two cues were available to listeners: envelope ITD and ongoing ITD. In this experiment, the envelope ITD was zero for all stimuli, and the ongoing ITD was varied, as shown in Fig. 2.19. Here, “envelope” refers to the shape of a gating function with 10-ms linear ramps at the onset and offset. Stimuli were presented binaurally to the left and right ears through plastic tubes and earpieces inserted into the ear canals. All signals were presented at 60 dB SPL, and the ILD was set to 0 dB.

Figure 2.20 shows the N1m ECD moment as a function of ITD. When the IACC of the stimulus was 0.95, the effect of ITD on the N1m amplitude, namely ECD moments, was significant. The N1m amplitude increased with increasing ITD in the right hemisphere in the case of a left-leading stimulus and in both the left and right hemispheres in the case of a right-leading stimulus. This result is consistent with previous findings (Sams et al. 1993; McEvoy et al. 1993; Palomäki et al. 2005). The N1m amplitude increased slightly with increasing ITDs in the hemisphere contralateral to the ITDs when the IACC of the stimulus was 0.5; however, the main effect of ITDs on the N1m amplitude was not significant. Lateralization performance worsens with decreasing IACCs (Jeffress et al. 1962; McEvoy et al. 1991; Zimmer

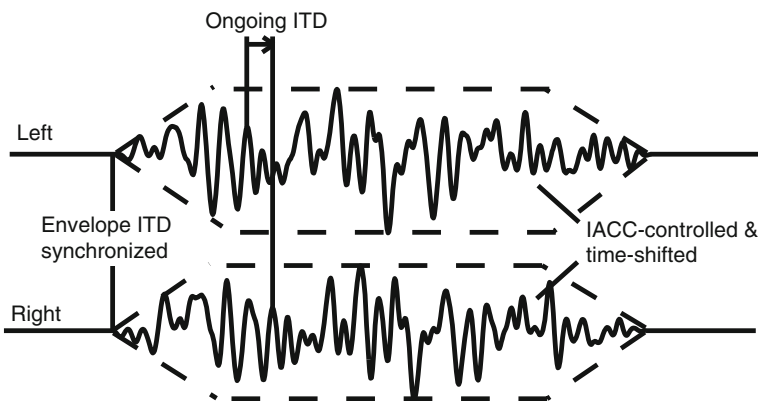
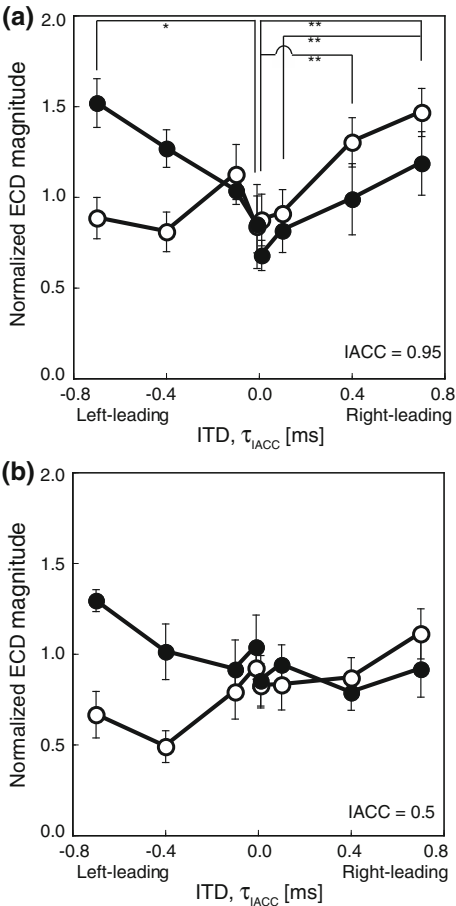


Fig. 2.19 Illustration of the stimuli used in the experiments. The fine structure (IACC controlled) of the stimulus was interaurally delayed, while the envelopes were synchronized between the ears

Fig. 2.20 Mean ECD moment of the N1m (\pm SEMs) as a function of the τ_{IACC} from the right (*filled circle*) and left (*open circle*) hemispheres when the IACC was 0.95 (a) and 0.5 (b). Asterisks indicate statistical significance (* $P < 0.05$, ** $P < 0.01$; Post hoc Newman-Keuls test) (Soeta and Nakagawa 2009)



and Macaluso 2005); therefore, the present results may indicate that lateralization performance is reflected in N1m amplitudes. Put another way, there is a close relationship between the N1m amplitudes and the IACCs and ITDs of the stimuli.

Previous research has indicated that the N1m amplitudes significantly decreased with increasing IACCs when the ITD of the stimulus was 0.0 ms (Soeta et al. 2004b). This result contradicts the present findings. The cortical response to the change in IACCs has recently been analyzed (Chait et al. 2005), and the results indicated that the strength of the response increases with the IACC difference and that the brain responses are more sensitive to the transition from an IACC of 1.0 than to the transition from an IACC of 0.0. That is, there are two factors that influence the cortical response regarding IACC: the transition from correlated or uncorrelated noise and the size of the IACC transition. Thus, the reason the N1m amplitudes did not decrease with increasing IACCs when the ITD of the stimulus

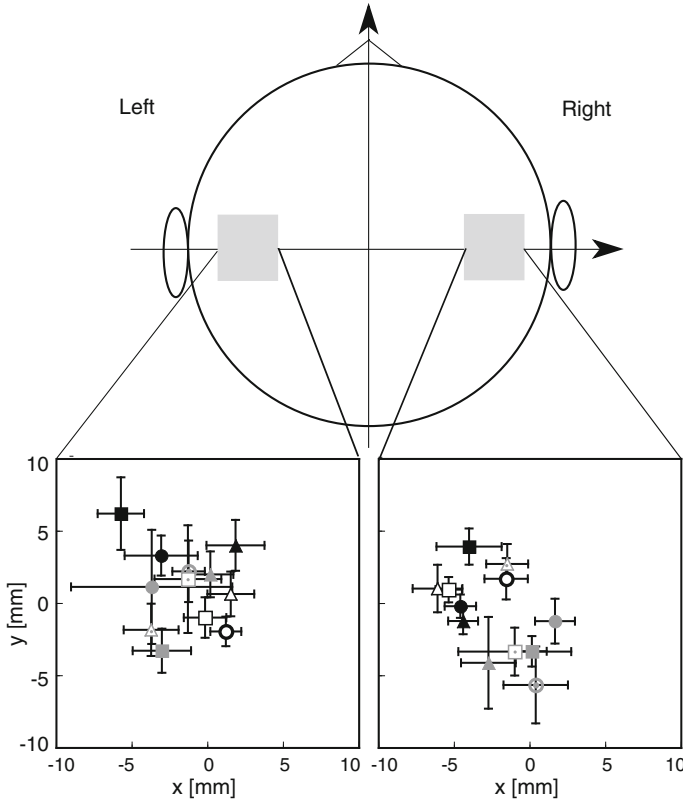


Fig. 2.21 Mean ECD location (\pm SEM) of all listeners in the *left* and *right* temporal planes when the IACC was 0.95 and 0.5. The ECD locations were normalized within each listener with respect to the position of ITD = 0.0 ms (Soeta and Nakagawa 2009)

was 0.0 ms in the present study could be due to an asymmetry between the adapting effect of the uncorrelated reference stimulus (IACC = 0.0) used in the present study, compared to the correlated reference stimulus (IACC = 1.0) used in the previous one (Soeta et al. 2004b).

Figure 2.21 shows the averaged ECD locations in the left and right hemispheres. The location of the ECDs underlying the N1m responses did not vary as a function of ITD or IACC, a finding in agreement with previous MEG results (McEvoy et al. 1993; Sams et al. 1993; Soeta et al. 2004b). As for Functional magnetic resonance imaging (fMRI), similarly, little evidence exists for segregated representations of specific ITDs or IACCs in auditory cortex (Woldorff et al. 1999; Maeder et al. 2001; Budd et al. 2003; Krumbholz et al. 2005; Zimmer and Macaluso 2005). Stimuli with different ITDs or IACCs may excite somewhat different neuronal populations, although the cortical source location did not differ systematically as a

function of ITD or IACC. Therefore, we conclude that the present data do not show an orderly representation of ITD or IACC in the human auditory cortex that can be resolved by MEG.

Recently, it has been suggested that ITDs may be coded by the activity level in two broadly tuned hemispheric channels (McAlpine et al. 2001; Brand et al. 2002; McAlpine and Grothe 2003; Stecker et al. 2005). The present study showed that the N1m amplitude varies with the ITD; however, the location of the ECDs underlying the N1m responses did not vary with the ITD. This could suggest that different ITDs are coded nontopographically but by response level. Thus, the current data seem to be more consistent with a two-channel model (McAlpine et al. 2001; Brand et al. 2002; McAlpine and Grothe 2003; Stecker et al. 2005) rather than a topographic representation model (e.g., Jeffress 1948).

2.4 Signal Processing Model of Human Auditory System

Based on the above-mentioned physiological responses, a central auditory signal processing model has been proposed (Ando 1998). The model consists of the autocorrelation mechanisms and the interaural cross-correlation mechanisms between the two auditory pathways for temporal and spatial factors of the sound field as shown in Fig. 2.22. In this figure, a sound source $p(t)$ is located at r_0 in a three-dimensional space, and a listener is sitting at r , which is defined by the location of the center of the head, $h_{l,r}(r|r_{0,r})$, being the impulse responses between r_0 and the left and right ear canal entrances. The impulse responses of the external ear canal and the bone chain are $e_{l,r}(t)$ and $c_{l,r}(t)$, respectively. The velocity of the basilar membrane is expressed by $V_{l,r}(x, \omega)$, with x being the position along the membrane.

The action potentials from the hair cells are conducted and transmitted to the cochlear nuclei, the SOC including the MSO, the LSO, and the trapezoid body, and to the higher level of the two cerebral hemispheres. The input power density spectrum of the cochlea $I(x')$ can be roughly mapped at a certain nerve position x' (Katsuki et al. 1958; Kiang et al. 1965) as a temporal activity. Amplitudes of waves (I–IV) of the ABR reflect the SPLs at both ears as a function of the horizontal angle of incidence to a listener. Such neural activities include sufficient information to attain the ACF at the LLN as indicated by $\Phi_{ll}(\sigma)$ and $\Phi_{rr}(\sigma)$. In fact, the time domain analysis of firing rate from the auditory nerve of cat revealed a pattern of ACF, but the frequency domain analysis did not (Secker-Walker and Searle 1990). Pooled interspike interval distributions resemble the short time or the running ACF for the low-frequency component as shown in Fig. 2.23 (Cariani 2001). It traces a change of the pitch as a function of the time. The pooled interval distributions for sound stimuli consisting of the high-frequency component resemble the envelope to running ACF (Cariani and Delgutte 1996a, b). From a viewpoint of the missing

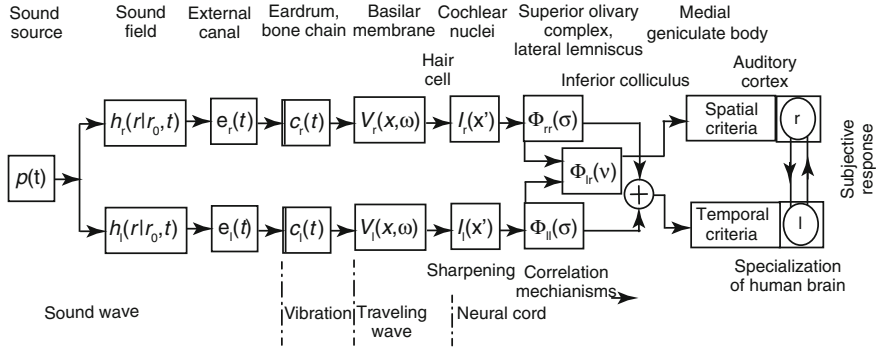


Fig. 2.22 Central auditory signal processing model for subjective responses. $p(t)$, source sound signal in the time domain; $h_{l,r}(r/r_0, t)$, head-related impulse responses from a source position of r_0 to the left and right ear entrances of a listener at r ; $e_{l,r}(t)$, impulse responses of left and right external canals from the left and right ear entrances to the left and right eardrums; $c_{l,r}(t)$, impulse responses for vibration of left and right bone chains from the eardrums to *oval* windows, including transformation factors into vibrational motion at the eardrums; $V_{l,r}(x, \omega)$, traveling wave forms on the basilar membranes, where x is the position along the left and right basilar membrane measured from the *oval* window; and $I_{l,r}(x')$, sharpening in the cochlear nuclei corresponding with roughly the power spectra of input sound (i.e., responses of a single pure tone ω tend to approach a limited region of nuclei). These neural activities may be enough to convert into activities similar to the ACF. $\Phi_{ll}(\sigma)$ and $\Phi_{rr}(\sigma)$: ACF mechanisms in the left and right auditory pathways, respectively. Symbol \oplus signifies that signals are combined. $\Phi_{lr}(v)$, IACF mechanism (Ando 1985); r and l , specialization for temporal and spatial factors of the left and right human cerebral hemispheres, respectively. Temporal sensations and spatial sensations may be processed in the left and right hemisphere according to the temporal factors extracted from the ACF and the spatial factors extracted from the IACF, respectively

fundamental or pitch of the complex tone judged by humans, the running ACF must be processed in the frequency components below about 5 kHz. The missing fundamental or pitch may be perceived less than about 1.2 kHz (Inoue et al. 2001), which may cover most musical signals. A tentative model of the running ACF processor is illustrated in Fig. 2.24. The output of the ACF processor may be dominantly connected with the left cerebral hemisphere.

As is also discussed, the neural activity (wave V together with waves IV_l and IV_r) may correspond to the IACC as shown in Fig. 2.16. Thus, the interaural cross-correlation mechanism may exist at the IC. It is concluded that the output signal of the interaural cross-correlation mechanism including the IACC may be dominantly connected to the right hemisphere. Also, the SPL expressed by a geometric average of the ACFs for the two ears at the origin of time ($\sigma = 0$) and in fact appears in the latency at the IC, and may be processed in the right hemisphere. The neural process has been developed realizing a minimum of effort and a maximum of efficiency, so that only information of criteria extracted from the ACF and IACF are transmitted into the left and right hemispheres, respectively.

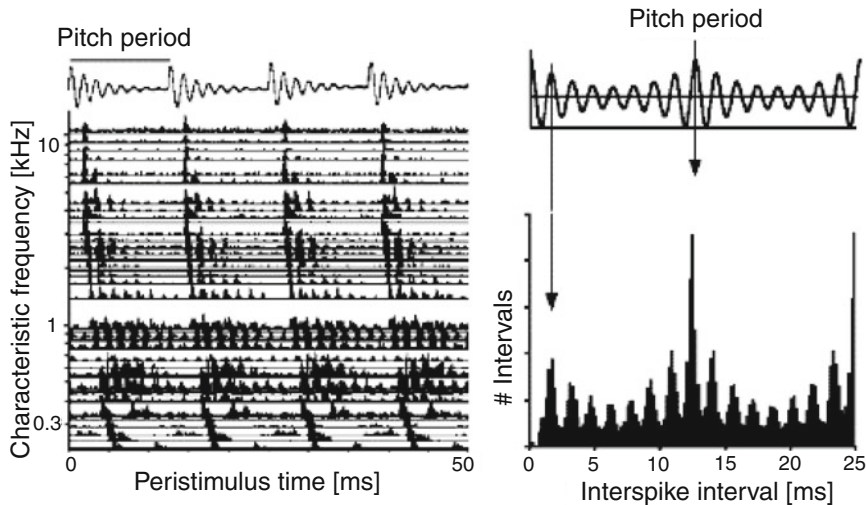


Fig. 2.23 *Top* stimulus waveform, single formant vowel, $F_0 = 80$ Hz, $F_1 = 640$ Hz, 60 dB SPL, 100 presentations/fiber. *Left* prestimulus time histograms of the responses of 53 auditory nerve fibers of Dial-anesthetized cats, arranged by fiber characteristic frequency. *Top right* stimulus ACF. *Bottom right* global ensemble-wide distribution of all-order interspike intervals. The most frequent interval in the distribution is 12.5 ms, which corresponds to the stimulus fundamental period ($1/F_0 = 1/80$ Hz) and the period of the low pitch that is heard (Cariani 2001)

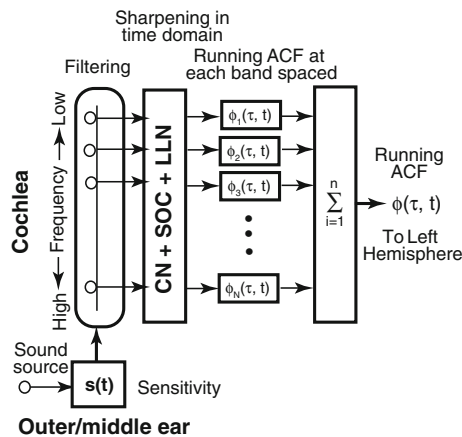


Fig. 2.24 A tentative two-dimensional model of the ACF processor in the auditory pathways. In the filtering process, however, there is no scientific evidence. The cutoff frequencies fixed, for example, might be arbitrary. Thus, it is considered that a kind of running window-filtering process in the frequency domain like the ACF analysis in the time domain might exist. In order to identify this process, a three-dimensional model might be considered, because the neuron distributes in the three-dimensional space

2.5 Brain Response in Relation to Loudness

The subjective aspect of sound intensity is loudness. Loudness is the attribute of auditory sensation in terms of which sounds may be ordered on a scale extending from quiet to loud. Loudness is what we experience in daily life. Someone can speak loudly or softly, and the volume of an audio device can be turned up or down. The mechanisms underlying the perception of loudness are not fully understood. The idea that loudness is simply proportional to the total number of action potentials fired by all auditory nerve neurons (the spike count hypothesis) has been investigated in animal studies. The spike count hypothesis was tested and justified that the rate of growth of both loudness and the auditory nerve spike count agreed over a wide range of tone intensity (Zwislocki 1965; Goldstein 1974; Lachs et al. 1984). However, disagreement also exists (Pickles 1983; Relkin and Doucet 1997).

The effect of sound intensity in the auditory cortex has been previously investigated by MEG, and AEF in response to stimulus intensity has been examined (e.g., Reite et al. 1982; Bak et al. 1985; Pantev et al. 1989; Vasama et al. 1995; Soeta and Nakagawa 2009). These results indicate that the N1m amplitude of the AEFs increases up to a stimulus intensity of 50–60 dB SPL, but then remains more or less constant or even decreases for higher intensities. The intensity dependence of the ECD location in human auditory cortex has also been examined. Pantev et al. (1989) reported that the higher the stimulus intensity is, the more superficial is the locus of cortical excitation. Vasama et al. (1995), however, failed to find any systematic variation of the N1m source locations as a function of intensity.

In previous studies on MEG response as a function of frequency, the ECD locations, that is, tonotopic organization, have been studied in considerable detail. Relatively, little research has been conducted on amplitude response as a function of frequency. The N1m response amplitude as a function of frequency has been examined using pure tones, and the results showed that the N1m amplitude peaks at 1000 Hz (Pantev et al. 1995). However, other researches have indicated that the N1m amplitude remains fairly constant, independent of test frequency (Pantev et al. 1988; Lütkenhöner et al. 2003).

Regarding the representation of noise in auditory cortex, auditory single-unit responses in the superior temporal gyrus of monkeys have been examined (Rauschecker et al. 1995; Rauschecker and Tian 2000; Lakatos et al. 2005). Responses of lateral neurons to band-pass noise are stronger than responses to pure tones. fMRI has showed that pure tones activate primarily the core, whereas band-pass noises activate preferably the belt areas in human auditory cortex (Wessinger et al. 2001). Relatively, little is known about the response amplitude in human auditory cortex as a function of frequency and bandwidth.

Changes in sound level are highly correlated with loudness changes; however, the relationship is not perfect. That is, changes in the frequency and bandwidth also affect the perceived loudness (Yost 2000). To evaluate the relationship between loudness and the activities of the auditory cortex, AEFs in response to the frequency and bandwidth were investigated (Soeta et al. 2006; Soeta and Nakagawa 2008b).

Octave band, 1/3 octave band, and 130 Hz bandwidth noises with center frequencies of 0.25, 0.5, 1, 2, 4, and 8 kHz were used as stimuli in Experiment 1 (Soeta et al. 2006). Pure tones, 1/6 octave band noise, and 1/3 octave band noise with center frequencies of 0.063, 0.125, 0.25, 0.5, 1, 2, 4, 8, 12, and 16 kHz were used in Experiment 2 (Soeta and Nakagawa 2008b). The octave band noises have fixed bandwidth in a logarithmic frequency scale. The 130 Hz bandwidth noises have fixed bandwidth irrespective of center frequency, such as pure tone. To make band-pass noises, the white noises were filtered using fourth-order Butterworth filters. Center frequencies of the noise bands are given as the geometric means of low- and high-frequency cutoffs. The stimulus duration was 500 ms, including rise and fall ramps of 10 ms. Stimuli were presented monaurally in Experiment 1 and binaurally in Experiment 2 through plastic tubes and earpieces inserted into the ear canals.

The AEFs were recorded using a 122-channel whole-head DC-SQUID (Neuromag-122TM) in a magnetically shielded room (Hämäläinen et al. 1993). To maintain a constant level of attention, listeners were instructed to concentrate on a self-selected silent movie projected on a screen in front of them and to ignore the auditory stimuli. The magnetic data were sampled at 400 Hz after being band-pass filtered between 0.03 and 100 Hz and then averaged. Responses were rejected if the magnetic field exceeded 3000 fT/cm in any channel. The averaged responses were digitally filtered between 1.0 and 30.0 Hz. The analysis time was 0.7 s from 0.2 s prior to the stimulus onset. The average of the 0.2-s prestimulus period served as the baseline. To evaluate the latency of the N1m peak, the RMSs of $\partial B_z / \partial x$ and $\partial B_z / \partial y$ were determined as the amplitude of the responses at each recording position. The amplitude and latency with maximum peak amplitude in the latency range from 70 to 160 ms over each left and right hemisphere were defined as the N1m amplitude and latency in each listener.

A psychophysical loudness experiment was carried out individually in an anechoic and soundproof room. A two-interval, two-alternative, forced-choice, adaptive procedure was employed to measure the point of subjective equality (PSE) in the loudness balance task (Levitt 1971; Jesteadt 1980; Schlauch and Wier 1987). In these two sequences, the upper sequence used a 2-down, 1-up decision rule to track the 71 % response level, while the lower sequence used a 1-down, 2-up decision rule to track the 29 % response level in Experiment 1. A simple 1-up, 1-down rule was adopted in Experiment 2. In each trial, a standard sound with a fixed level and a comparison sound with a variable level that was selected randomly from one of two sequences were presented randomly in either the first interval or the second interval. The comparison stimulus was the 1000-Hz tone, and the two intervals were separated by 500 ms. The listener's task was to indicate which sound was louder by pressing a key. Each sequence was terminated by having reached 10 or 12 reversals. The level at which a reversal occurred was recorded, and the last four reversals were averaged at the end of the run to estimate the 71 and 29 % response levels. The PSE was estimated as the average of the 71 % and the 29 % levels in Experiment 1. The arithmetic mean of the last four of the levels was used to estimate the PSE in Experiment 2.

Figure 2.25 shows mean N1m amplitude plotted as a function of center frequency in Experiment 1. The main effect of the center frequencies on the N1m amplitude was significant for all bandwidth. Regarding 1/3 octave band noise, middle frequency range stimuli (500–2000 Hz) appear to be associated with larger amplitude. Regarding 130 Hz bandwidth noise, the maximum amplitude was found in the center frequency of 1000 Hz.

Figure 2.26 shows mean N1m latency plotted as a function of center frequency in Experiment 1. Middle frequency range stimuli (1000–4000 Hz) appear to be associated with shorter N1m latencies for all bandwidth. Lower and higher frequency stimuli give rise to relatively delayed N1m responses.

Figure 2.27 shows mean N1m amplitude plotted as a function of center frequency in Experiment 2. The N1m amplitude showed peaks at around 0.5 and 1 kHz, and decreased with decreasing center frequency at lower frequencies and decreased with increasing center frequency at higher frequencies. This tendency is consistent with previous studies using pure tones (Pantev et al. 1995; Fujioka et al. 2003) and band-pass noise (Soeta et al. 2006). The main effect of the center frequency on the N1m amplitude was significant ($p < 0.05$).

Figure 2.28 shows mean N1m latency plotted as a function of center frequency in Experiment 2. The latency of the N1m had minima between around 1 and 4 kHz. Middle frequency range sounds (1–4 kHz) appear to be associated with shorter N1m latencies. Lower and higher frequency stimuli had relatively delayed N1m responses. This is consistent with previous studies using pure tones (Roberts and Poeppel 1996; Stufflebeam et al. 1998; Lütkenhöner et al. 2001) and band-pass noise (Soeta et al. 2006).

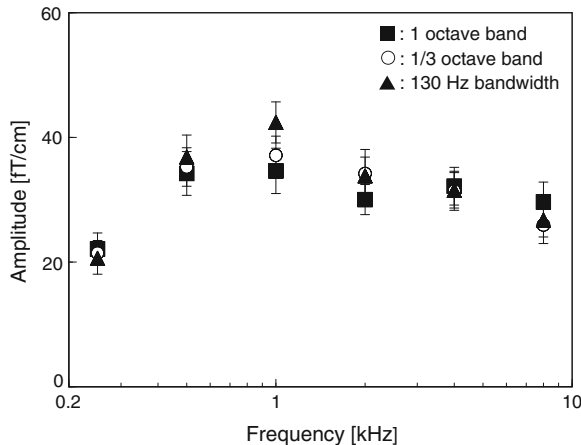


Fig. 2.25 Mean amplitude of the N1m (\pm SEMs) from both left and right hemispheres in response to (filled square) 1 octave band, (open circle) 1/3 octave band, and (filled triangle) 130 Hz bandwidth noises as a function of the center frequencies

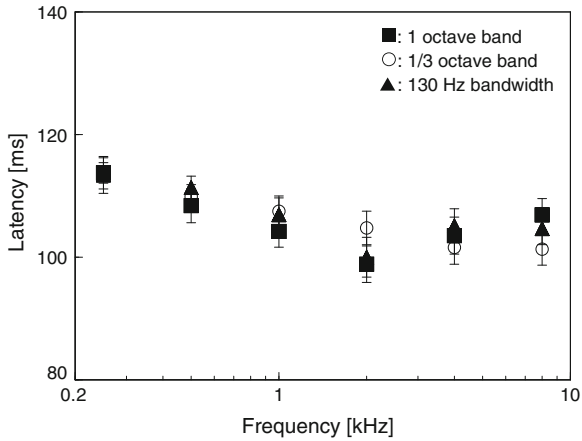
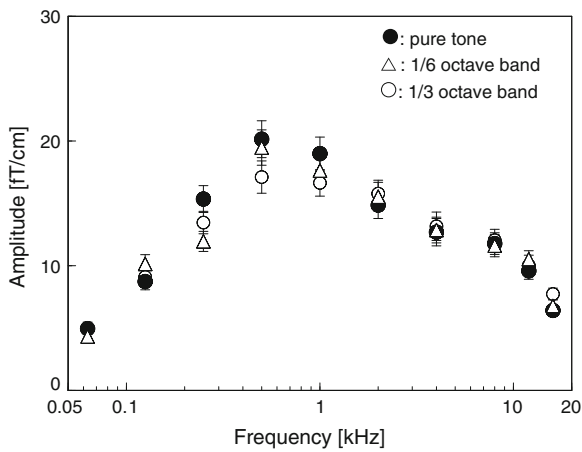


Fig. 2.26 Mean latency of the N1m (\pm SEMs) from both left and right hemispheres in response to (filled square) 1 octave band, (open circle) 1/3 octave band, and (filled triangle) 130 Hz bandwidth noises as a function of the center frequencies

Fig. 2.27 Mean amplitude of the N1m (\pm SEMs) from both left and right hemispheres as a function of the center frequency. The bandwidth indicated by (filled circle) pure tone, (open triangle) 1/6 octave band, and (open circle) 1/3 octave band



The averaged data for the loudness balance experiment are shown in Fig. 2.29. For comparison, loudness, which is drawn based on an equal loudness contour from Suzuki and Takeshima (2004) when SPL is 60 dB, is reproduced as the solid line. Correlation coefficients between loudness values and mean N1m amplitudes are listed in Table 2.1. The mean N1m amplitude correlated well to the loudness values in the center frequency below 2 kHz in both Experiments 1 and 2. The phase-locking might be important for the perception of loudness and the precision of phase-locking decreases with increasing frequency above 1–2 kHz (Carlyon and Moore 1984). The low correlation between loudness values and N1m amplitude in

Fig. 2.28 Mean latency of the N1m (\pm SEMs) from both left and right hemispheres as a function of the center frequency. The bandwidth indicated by (*filled circle*) pure tone, (*open triangle*) 1/6 octave band, and (*open circle*) 1/3 octave band

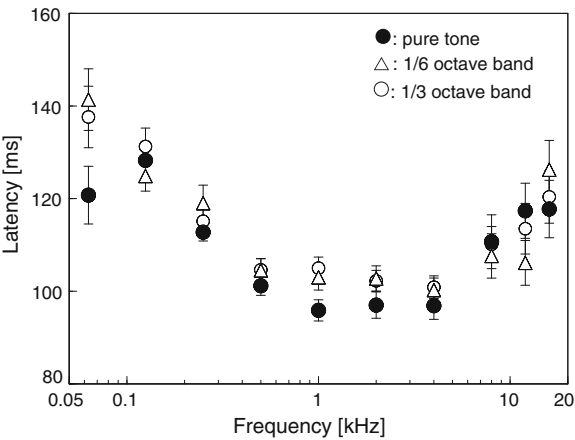


Fig. 2.29 Averaged loudness balance data between a 1000-Hz comparison tone (y-axis) and a standard sound as a function of the center frequency (x-axis) for (*filled square*) 1 octave band, (*open circle*) 1/3 octave band, and (*filled triangle*) 130 Hz bandwidth stimuli in (a) Soeta et al. (2006) and for (*filled circle*) pure tone, (*open triangle*) 1/6 octave band, and (*open circle*) 1/3 octave band stimuli in (b) Soeta and Nakagawa (2008b). Loudness when sound pressure level is 60 dB, which is drawn based on an equal loudness contour (Suzuki and Takeshima 2004), is represented by the solid line

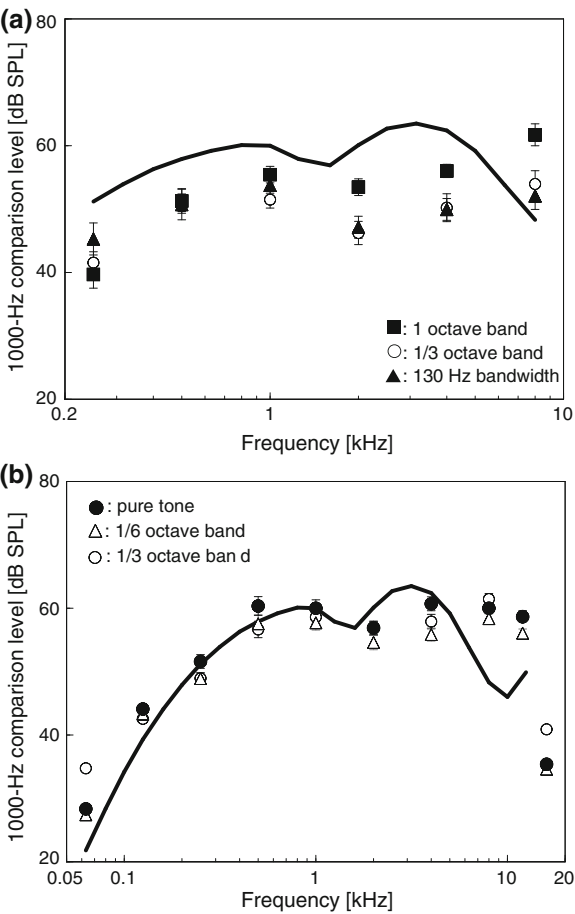
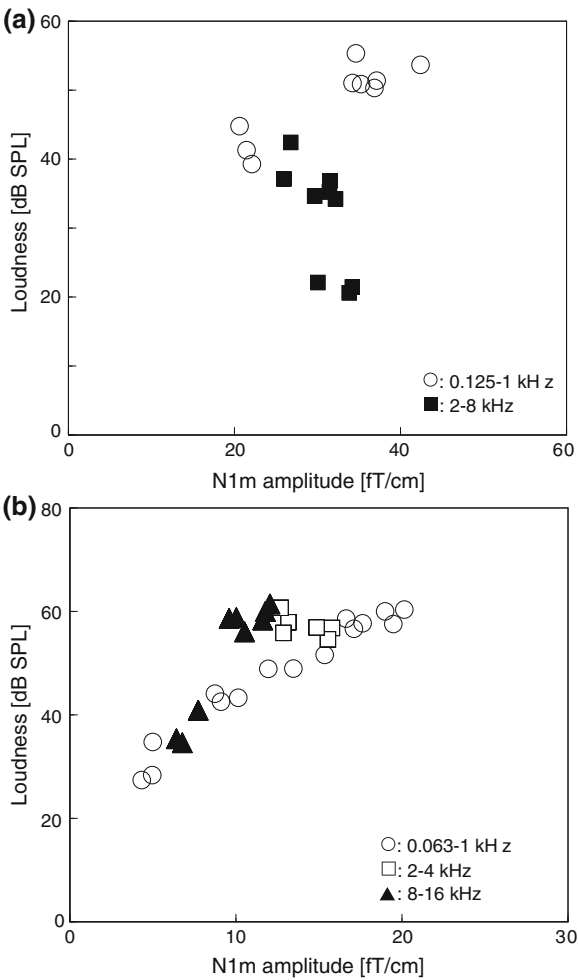


Table 2.1 Correlation coefficient between loudness values and N1m amplitudes

	All frequency range	Lower frequency range (<2 kHz)	Middle frequency range (2–8 kHz)	High frequency range (8 kHz–)
Experiment 1	0.47	0.78	–0.48	
Experiment 2	0.78	0.97	–0.71	0.96

the center frequency between 2 and 8 kHz might be due to the loss of phase-locking. Scatter-plot of loudness as a function of the N1m amplitude is shown in Fig. 2.30. In the high-frequency range (>8 kHz), the amplitude of the N1m also correlated well with loudness. However, no AEF responses correlated with loudness in the frequency around 2 and 4 kHz. The activation of neurons in human auditory cortices shows a more rapid growth with SPL for a low-frequency tone

Fig. 2.30 Scatter plot of loudness as a function of the N1m amplitude in the center frequency range of **a** 250–2000 Hz (Soeta et al. 2006) and **b** 63–16,000 Hz (Soeta and Nakagawa 2008b)



than for a high-frequency tone (Hart et al. 2003). The present results indicated that the amplitudes of the N1m show a more rapid growth with loudness for lower frequency stimuli (<2 kHz) than for higher frequency stimuli (>8 kHz). The transition of the growth in activation of the human auditory cortex from low to high frequency might be between 2 and 8 kHz.

The ear does not transmit all frequencies equally. That is, it does not have a flat frequency response. The outer ear modifies the sound waves in transferring the acoustic vibrations to the eardrum. The resonances of the external ear increase the sound pressure at the eardrum, particularly in frequency range of 2–7 kHz (Wiener and Ross 1946; Shaw and Teranishi 1968; Shaw 1974; Mehrgardt and Mellert 1977). In other words, the transfer function from a sound source to the eardrum, which can be obtained by multiplying the HRTF between a sound source and the ear entrance, $H(\omega)$, and the function from the entrance to the eardrum, $E(\omega)$, together, has a broad peak at approximately 2.5 kHz. The middle ear apparatus then transfers the sound vibrations from eardrum to the cochlea. The transfer function of the human middle ear, $C(\omega)$, can also be calculated and measured (Onchi 1961; Zwislocki 1962; Rubinstein et al. 1966; Nedzelnitsky 1980; Wada et al. 1992). It has band-pass characteristics, with greatest transmission being seen around 1 kHz. The transfer function between a sound source and the cochlea may be represented by $S(\omega) = H(\omega)E(\omega)C(\omega)$. It has a broad maximum near 3 kHz, and the pattern of the transfer function agrees with the ear sensitivity for people with normal hearing ability (Ando 1998). The N1m amplitudes derived from the 1/3 octave band and 130 Hz bandwidth noises (Fig. 2.25) appear similar to the transfer function of the human middle ear, $C(\omega)$, (Fig. 2.3).

2.6 Brain Response Corresponding to Annoyance

Basically, psychoacoustic annoyance depends on the loudness, timbre, and temporal structure of sounds. Loudness and annoyance have been distinguished and defined (Berglund et al. 1975; Hellman 1982). These authors relate annoyance to an individual's reaction to noise within the context of a given situation and loudness directly to sound intensity. Environmental noise has been related to annoyance in several studies (e.g., Rylander et al. 1972, 1980, 1986; Björkman and Björkman 1997; Rylander and Björkman 1997). It is generally recognized that loudness is the most influential determinant for annoyance and can be predicted by the SPL. Previous studies have concluded that perceived loudness remains constant with increasing noise bandwidth until the bandwidth reaches the critical band. Loudness then increases with increasing bandwidth at the same SPL (Zwicker et al. 1957; Greenwood 1961a, b; Scharf 1962). However, the loudness of a sharply filtered noise increases as the effective duration of the ACF, τ_e , increases, even when the bandwidth of the signal is within the critical band (Merthayasa et al. 1994; Sato et al. 2002; Soeta et al. 2004c). The τ_e represents repetitive features within the signal itself and increases as the filter bandwidth decreases. In addition, a sound is

perceived to be annoying although the SPL was only about 35 dBA in a given situation (Kitamura et al. 2002). This demonstrates that annoyance cannot be predicted by sound intensity alone.

To investigate the relationship between the human brain and the environment, studies were made using EEG and MEG. To investigate the relationship between the EEG responses and subjective preferences for a sound field, a method was developed using the ACF of EEG (Ando and Chen 1996; Chen and Ando 1996; Sato et al. 2003). The effective duration of the normalized ACF, τ_e , was analyzed with variation in the time delay of the single echo, Δt_1 , reverberation time (RT), and IACC of sound fields. Their results showed that the τ_e is significantly longer in preferred conditions for the factors, Δt_1 , RT, and IACC. It has also found that the τ_e and the maximum amplitude of the cross-correlation function (CCF), $|\phi(\tau)|_{\max}$, of MEG between 8 and 13 Hz is correlated with subjective preference for Δt_1 and IACC of speech signal (Soeta et al. 2002, 2003).

We investigated the responses of the human brain that correspond to noise annoyance (Soeta et al. 2004c). The scale values of annoyance for each listener were obtained by paired-comparison tests. MEG measurements and analyses by the ACF and CCF were made. The relationship between the scale value of annoyance to band-pass noise and the factors extracted from the ACF and CCF of MEG in the brain's magnetic responses were investigated.

Pure tone and band-pass noises with a center frequency of 1000 Hz were used as auditory signals. The bandwidth of the signal was set to 0, 40, 80, 160, or 320 Hz with a 2000 dB/octave sharp filter, obtained by a digital FFT filter, to control the ACF of the source signal (Sato et al. 2002). The filter bandwidth of 0 Hz was the only slope component. The auditory stimuli were binaurally delivered through plastic tubes and earpieces inserted into the ear canals. The sound pressure was measured with an ear simulator, including a microphone and a preamplifier, and an adaptor connected to the earpiece. All stimuli were fixed at the same SPL (74 dBA). The signals were characterized by ACF factors, τ_e , τ_1 , and ϕ_1 . The measured τ_1 of all signals were 1.0 ms, which correspond to the center frequency of band-pass noise. The measured ϕ_1 and τ_e increased as the filter bandwidth decreased with a certain degree of coherence between ϕ_1 and τ_e .

Seven listeners took part in the experiment, 22–28 year old with normal hearing. They were seated in a dark soundproof room, with a comfortable thermal environment, and were presented the sound stimuli. A paired-comparison tests were performed for all combinations of the pairs of pure tone and band-pass noise, i.e., 15 pairs ($N(N-1)/2$, $N=6$) of stimuli with interchange of the order of each pair per session and random presentation of the pairs. Ten sessions was conducted for each listener. The duration of the stimuli was 2.0 s, the rise and fall times were 10 ms, the silent interval between the stimuli was 1.0 s, and the interval between pairs was 4.0 s, which was the allowed time for the listeners to respond by pushing one of two buttons. They were asked to judge which of the two sound stimuli was more annoying. The scale values of the annoyance were calculated according to Case V of Thurstone's theory (Thurstone 1927; Gullikson 1956), and the model of Case V for all data was confirmed by the goodness-of-fit test (Mosteller 1951).

The same listeners joined in the annoyance tests took part in the recording of MEG responses. The magnetic responses were measured in a magnetically shielded room and recorded (passband 0.03–100 Hz, sampling rate 400 Hz) with a 122 channel whole-head DC-SQUID magnetometer. For the measurements, the listeners were seated in a dark soundproof room with a comfortable thermal environment and were asked to close their eyes and fully concentrate on the sound stimulus. The paired-auditory stimuli were presented in the same way as in the subjective annoyance test. Combinations of a reference stimulus (pure tone) and test stimuli (band-pass noise) were presented alternately 30 times at a constant 2.0-s inter-stimulus interval and MEGs recorded. Eighteen channels that were located around the temporal area in each hemisphere were selected for ACF and CCF analysis (Fig. 2.31). This resulted of 36 channels selected to be analyzed. Each response, corresponding to one stimulus, was analyzed by ACF and CCF for each listener. The relationship between the degree of annoyance and the averaged τ_e values at 18 sites, measured at two tangential derivatives, was investigated.

The ACF provides the same information as the power spectral density of a signal. Figure 2.32a shows an example of a measured ACF. A normalized ACF can be expressed by:

$$\phi(\tau) = \frac{\Phi(\tau)}{\Phi(0)}, \quad (2.3)$$

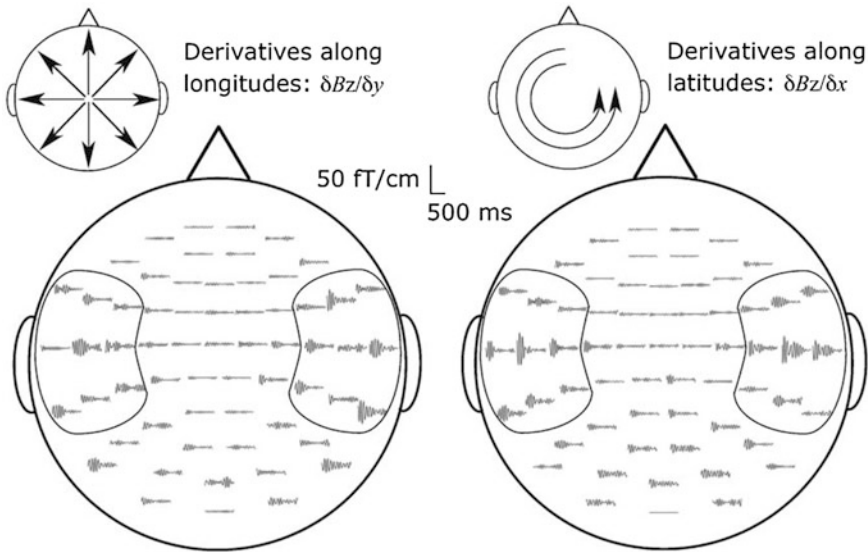


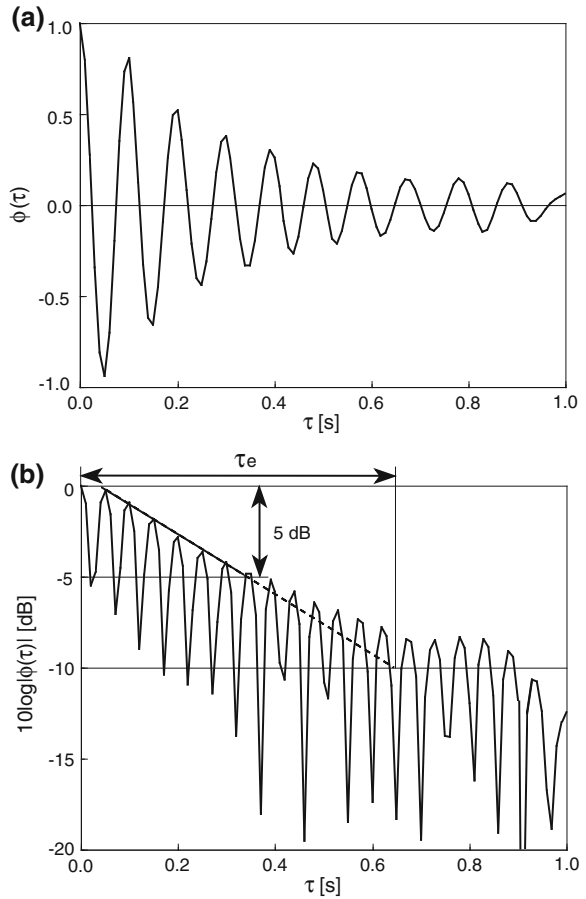
Fig. 2.31 Examples of recorded MEG responses to band-pass noise. The passband is 8–13 Hz. 36 channels that were located around the left and temporal area were selected for the ACF and CCF analysis (Soeta et al. 2004c)

where

$$\Phi(\tau) = \frac{1}{2T} \int_0^{2T} \alpha(t)\alpha(t+\tau)dt, \quad (2.4)$$

where $2T$ is the integral interval, τ is the time delay, and $\alpha(t)$ is the MEG between 8 and 13 Hz. Figure 2.32b shows the absolute value of the ACF in a logarithmic form as a function of the time delay, τ . To calculate the degree of the ACF envelope decay, the effective duration, τ_e , is determined. As shown in Fig. 2.32b, a straight-line regression of the ACF can only be made by using the initial declining portion, $0 \text{ dB} > 10 \log|\Phi(\tau)| > -5 \text{ dB}$ (Ando and Chen 1996). In most cases, the envelope decay of the initial part of the ACF may fit a straight line. The values of τ_e were analyzed at $2T = 2.0 \text{ s}$. Given the two signals are $\alpha_1(t)$ and $\alpha_2(t)$, then the CCF is defined by:

Fig. 2.32 **a** Examples of normalized ACF of MEGs between 8 and 13 Hz. **b** Examples of determining the effective duration of ACF, τ_e (Soeta et al. 2004c)



$$\Phi_{12}(\tau) = \frac{1}{2T} \int_{-T}^{+T} \alpha_1(t) \alpha_2(t + \tau) dt. \quad (2.5)$$

The normalized CCF is given by:

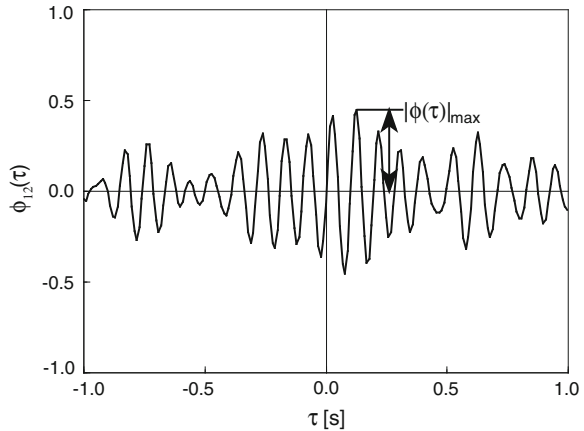
$$\phi_{12}(\tau) = \frac{\Phi_{12}(\tau)}{\sqrt{\Phi_{11}(0)\Phi_{22}(0)}}, \quad (2.6)$$

where $\Phi_{11}(0)$ and $\Phi_{22}(0)$ are the ACFs of $\alpha_1(t)$ and $\alpha_2(t)$ at $\tau = 0$, respectively. The normalized CCF between the MEG responses was recorded at the reference channels, with 18 channels for each hemisphere, and those recorded at the 35 test channels (with the exception of the reference channel) were calculated. Examples of a normalized CCF and the definition of the maximum value of the CCFs, $|\phi(\tau)|_{\max}$, are shown in Fig. 2.33. The values of $|\phi(\tau)|_{\max}$ were analyzed at $2T = 2.0$ s.

The values of τ_e for the most annoying stimuli were significantly shorter than those for the least annoying stimuli in six listeners ($p < 0.05$, one-way ANOVA). Figure 2.34a shows the relationship between the ratio of averaged values of τ_e of band-pass noise to those of a pure tone, and the difference between the scale values of band-pass noise and those of a pure tone. The ratio of τ_e increases as the difference of scale values of annoyance decreased (except for one listener). This indicates that the value of τ_e became shorter during the presentation of an annoying stimulus. The correlation coefficient between the ratio of τ_e values and the difference in scale values of annoyance was -0.83 ($p < 0.01$).

The results from the reference channel with the highest correlation between the scale values of annoyance and averaged $|\phi(\tau)|_{\max}$ values of all test channels showed a significant effect of the stimulus on $|\phi(\tau)|_{\max}$ values ($p < 0.001$). The values of $|\phi(\tau)|_{\max}$ for the most annoying stimuli were significantly smaller than those for the

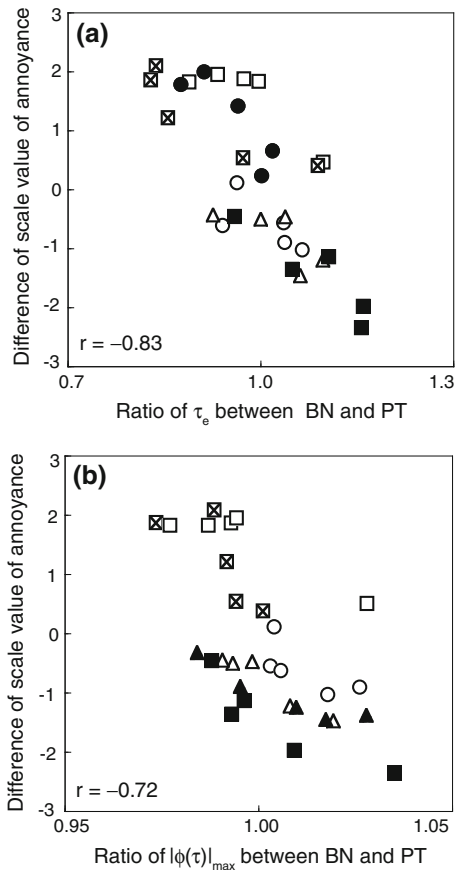
Fig. 2.33 Examples of normalized CCF of MEGs between 8 and 13 Hz and the definitions of the maximum value of CCF, $|\phi(\tau)|_{\max}$ (Soeta et al. 2004c)



least annoying stimuli for six listeners ($p < 0.001$, one-way ANOVA). The results indicate that the ratio of $|\phi(\tau)|_{\max}$ increases as the difference of scale values of annoyance decrease (except for one listener), as shown in Fig. 2.34b. This indicates that the value of $|\phi(\tau)|_{\max}$ becomes smaller during the presentation of an annoying stimulus. The correlation coefficient between the ratio of $|\phi(\tau)|_{\max}$ value and the difference in scale values of annoyance was -0.72 ($p < 0.01$).

The value of τ_e becomes shorter and the values of $|\phi(\tau)|_{\max}$ becomes smaller during presentation of an annoying stimulus. The τ_e is the degree of similar repetitive features included in MEG between 8 and 13 Hz, and the $|\phi(\tau)|_{\max}$ signifies the degree of similar repetitive features that appear in MEG between 8 and 13 Hz recorded at two different channels. Thus, the brain is unstable over a wider range, in both space and time during annoying conditions. Previous studies on EEG and MEG between 8 and 13 Hz show that the τ_e becomes significantly longer and $|\phi(\tau)|_{\max}$ significantly larger in preferred sound fields (Ando and Chen 1996; Chen and Ando 1996; Sato et al. 2003; Soeta et al. 2002, 2003). This indicates that the

Fig. 2.34 Relationship between the difference of scale values (SV) [SV (band-pass noise) – SV (pure tone)] and the ratio of **a** τ_e and **b** $|\phi(\tau)|_{\max}$ values of band-pass noise (BN) to those of a pure tone (PT). Each symbol represents one listener



brain repeats a similar rhythm over a wider range, in both space and time in preferred conditions. These are considered to be consistent with the present results.

Alpha activity is commonly defined as fluctuations between 8 and 13 Hz that can be detected on the occipital scalp (Chapman et al. 1984). Similar oscillatory activity, seen over the auditory cortex, is called τ rhythm (Tiihonen et al. 1991; Dinse et al. 1997). It is this τ rhythm that is analyzed by the ACF and CCF in this study. The high correlation between annoyance and the values of τ_e and $|\phi(\tau)|_{\max}$ was not found in other frequency bands, such as delta (1–4 Hz), theta (4–8 Hz), and beta (13–30 Hz).

References

- Aibara R, Welsh JT, Puria S, Goode RL (2001) Human middle-ear sound transfer function and cochlear input impedance. *Hear Res* 152:100–109
- Albeck Y, Konishi M (1995) Responses of neurons in the auditory pathway of the barn owl to partially correlated binaural signals. *J Neurophysiol* 74:1689–1700
- Ando Y (1985) Concert hall acoustics. Springer, Heidelberg
- Ando Y (1998) Architectural acoustics: blending sound sources, sound fields, and listeners. AIP Press/Springer, New York
- Ando Y (2001) A theory of primary sensations and spatial sensations measuring environmental noise. *J Sound Vib* 241:3–18
- Ando Y (2002) Correlation factors describing primary and spatial sensations of sound fields. *J Sound Vib* 258:405–417
- Ando Y, Chen C (1996) On the analysis of autocorrelation function of a-waves on the left and right cerebral hemispheres and in relation to the time delay of single sound reflection. *J Architec Plan Env Eng* 488:67–73
- Ando Y, Hosaka I (1983) Hemispheric difference in evoked potentials to spatial sound field stimuli. *J Acoust Soc Am* 74(S1):S64–S65
- Ando Y, Kang SH, Nagamatsu H (1987) On the auditory-evoked potentials in relation to the IACC of sound field. *J Acoust Soc Jpn (E)* 8:183–190
- Ando Y, Yamamoto K, Nagamatsu H, Kang SH (1991) Auditory brainstem response (ABR) in relation to the horizontal angle of sound incidence. *Acoust Lett* 15:57–64
- Ando Y, Sato S, Sakai H (1999) Fundamental subjective attributes of sound fields based on the model of auditory brain system. In: Sendra JJ (ed) *Computational acoustics in architecture*. WIT Press, Southampton, pp 63–99
- Bak CK, Lebech J, Saermark K (1985) Dependence of the auditory evoked magnetic field (100 msec signal) of the human brain on the intensity of the stimulus. *Electroenceph Clin Neurophysiol* 61:141–149
- Berglund B, Berglund U, Lindvall T (1975) Scaling loudness, noisiness, and annoyance of aircraft noise. *J Acoust Soc Am* 57:930–934
- Bilsen FA (1966) Repetition pitch: monaural interaction of a sound with the repetition of the same, but phase shifted sound. *Acustica* 17:295–300
- Bilsen FA, Ritsma RJ (1969) Repetition pitch and its implication for hearing theory. *Acustica* 22:63–73
- Bilsen FA, ten Kate JH, Buunen TJF, Raatgever J (1975) Responses of single units in the cochlear nucleus of the cat to cosine noise. *J Acoust Soc Am* 58:858–866
- Björkman M, Rylander R (1997) Maximum noise levels in city traffic. *J Sound Vib* 205:513–516
- Blauert J (ed) (1996) *Spatial hearing*. The MIT Press, Cambridge

- Blauert J, Lindemann W (1986) Spatial mapping of intracranial auditory events for various degrees of interaural coherence. *J Acoust Soc Am* 79:806–813
- Brand A, Behrend O, Marquardt T, McAlpine D, Grothe B (2002) Precise inhibition is essential for microsecond interaural time difference coding. *Nature* 417:543–547
- Budd TW, Hall DA, Gonçalves MS, Akeroyd MA, Foster JR, Palmer AR, Head K, Summerfield AQ (2003) Binaural specialisation in human auditory cortex: an fMRI investigation of interaural correlation sensitivity. *Neuroimage* 20:1783–1794
- Butler RA, Belundiuk K (1977) Spectral cues utilized in the location of sound in the median sagittal plane. *J Acoust Soc Am* 61:1264–1269
- Cansino S, Ducorps A, Ragot R (2003) Tonotopic cortical representation of periodic complex sounds. *Hum Brain Mapp* 20:71–81
- Cariani PA (2001) Neural timing nets. *Neural Netw* 14:737–753
- Cariani PA, Delgutte B (1996a) Neural correlates of the pitch of complex tones. I. Pitch and pitch salience. *J Neurophysiol* 76:1698–1716
- Cariani PA, Delgutte B (1996b) Neural correlates of the pitch of complex tones. II. Pitch shift, pitch ambiguity, phase invariance, pitch circularity, rate pitch, and the dominance region for pitch. *J Neurophysiol* 76:1717–1734
- Carlyon RP, Moore BCJ (1984) Intensity discrimination: a severe departure from Weber's law. *J Acoust Soc Am* 76:1369–1376
- Chait M, Poeppel D, Cheveigne A, Simon JZ (2005) Human auditory cortical processing of changes in interaural correlation. *J Neurosci* 25:8518–8527
- Chandrasekaran B, Kraus N (2010) The scalp-recorded brainstem response to speech: neural origins and plasticity. *Psychophysiology* 47:36–246
- Chapman RM, Ilmoniemi RJ, Barbanera S, Romani GL (1984) Selective localization of alpha brain activity with neuromagnetic measurements. *Electroencephalogr Clin Neurophysiol* 58:569–572
- Chen C, Ando Y (1996) On the relationship between the autocorrelation function of a-waves on the left and right cerebral hemispheres and subjective preference for the reverberation time of music sound field. *J Architec Plan Env Eng* 489:73–80
- Colburn HS (1977) Theory of binaural interaction based on auditory-nerve data. II. Detection of tones in noise. *J Acoust Soc Am* 61:525–533
- D'Angelo WR, Sterbing SJ, Ostapoff EM, Kuwada S (2003) Effects of amplitude modulation on the coding of interaural time differences of low-frequency sounds in the inferior colliculus. II. Neural mechanisms. *J Neurophysiol* 90:2827–2836
- Denham S (2005) Pitch detection of dynamic iterated rippled noise by humans and a modified auditory model. *Biosystems* 79:199–206
- Dinse HR, Krüger K, Akhavan AC, Spengler F, Schüner G, Schreiner CE (1997) Low-frequency oscillations of visual, auditory and somatosensory cortical neurons evoked by sensory stimulation. *Int J Psychophysiol* 26:205–227
- Elberling C, Bak C, Kofoed B, Lebech J, Sarmark G (1982) Auditory magnetic fields from the human cerebral cortex: location and strength of an equivalent current dipole. *Acta Neurol Scand* 65:553–569
- Fastl H, Stoll G (1979) Scaling of pitch strength. *Hear Res* 1:293–301
- Fay RR, Yost WA, Coombs S (1983) Psychophysics and neurophysiology of repetition noise processing in a vertebrate auditory system. *Hear Res* 12:31–55
- Fujioka T, Ross B, Okamoto H, Takeshima Y, Kakigi R, Pantev C (2003) Tonotopic representation of missing fundamental complex sounds in the human auditory cortex. *Eur J Neurosci* 18:432–440
- Gardner MB, Gardner RS (1973) Problem of localization in the median plane: Effect of pinna cavity occlusion. *J Acoust Soc Am* 53:400–408
- Goldstein JL (1974) Is the power law simply related to the driven spike response rate from the whole auditory nerve? In: Moskowitz HR, Scharf B, Stevens JC (eds) *Sensation and measurement*. Reidel, Dordrecht, pp 223–229
- Greenwood DD (1961a) Auditory masking and the critical band. *J Acoust Soc Am* 33:484–502

- Greenwood DD (1961b) Critical bandwidth and the frequency of the basilar membrane. *J Acoust Soc Am* 33:1344–1356
- Gullikson H (1956) A least squares solution for paired comparisons with incomplete data. *Psychometrika* 21:125–134
- Hämäläinen MS, Hari R, Ilmoniemi RJ, Knuutila J, Lounasmaa OV (1993) Magnetoencephalography? Theory, instrumentation, and applications to noninvasive studies of the working human brain. *Rev Mod Phys* 65:413–497
- Hart HC, Hall DA, Palmer AR (2003) The sound-level-dependent growth in the extent of fMRI activation in Heschl's gyrus is different for low- and high-frequency tones. *Hear Res* 179:104–112
- Hellman RP (1982) Loudness, annoyance and noisiness produced by single-tone-noise complexes. *J Acoust Soc Am* 72:62–73
- Inoue M, Ando Y, Taguti T (2001) The frequency range applicable to pitch identification based upon the autocorrelation function model. *J Sound Vib* 241:105–116
- ISO 226:2003 Acoustics—normal equal-loudness-level contours
- Jeffress LA (1948) A place theory of sound localization. *J Comp Physiol Psych* 61:468–486
- Jeffress LA, Blodgett HC, Deatherage BH (1962) Effects of interaural correlation on the precision of centering a noise. *J Acoust Soc Am* 34:1122–1123
- Jesteadt W (1980) An adaptive procedure for subjective judgments. *Percept Psychophys* 28:85–88
- Katsuki Y, Sumi T, Uchiyama H, Watanabe T (1958) Electric responses of auditory neurons in cat to sound stimulation. *J Neurophysiol* 21:569–588
- Kaukoranta E, Hämäläinen M, Sarvas J, Hari R (1986) Mixed and sensory nerve stimulations activate different cytoarchitectonic areas in the human primary somatosensory cortex SI: Neuromagnetic recordings and statistical considerations. *Exp Brain Res* 63:60–66
- Keller CH, Takahashi TT (1996) Binaural cross-correlation predicts the responses of neurons in the owl's auditory space map under conditions simulating summing localization. *J Neurosci* 16:4300–4309
- Kiang NYS, Watanabe T, Thomas EC, Clark LF (1965) Discharge patterns of single fibers in the cat's auditory nerve. MIT Press, Cambridge
- Kitamura T, Sato S, Shimokura R, Ando Y (2002) Measurement of temporal and spatial factors of a flushing toilet noise in a downstairs bedroom. *J Temporal Des Arch Environ* 2:13–19
- Knuutila J, Ahonen A, Hämäläinen M, Kajola M, Laine P, Lounasmaa O, Parkkonen L, Simola J, Tesche C (1993) A 122-channel whole cortex SQUID system for measuring the brain's magnetic fields. *IEEE Trans Magn* 29:3315–3320
- Krishnan A (2007) Human frequency following response. In Burkard RF, Don M, Eggermont JJ (eds) *Auditory evoked potentials: basic principles and clinical application*, Lippincott Williams & Wilkins, Baltimore, pp 313–335
- Krishnan A, Bidelman GM, Gandour JT (2010) Neural representation of pitch salience in the human brainstem revealed by psychophysical and electrophysiological indices. *Hear Res* 268:60–66
- Krishnan A, Xu Y, Gandour J, Cariani P (2005) Encoding of pitch in the human brainstem is sensitive to language experience. *Brain Res Cogn Brain Res* 25:161–168
- Krumbholz K, Patterson RD, Seither-Preisler A, Lammertmann C, Lütkenhöner B (2003) Neuromagnetic evidence for a pitch processing center in Heschl's gyrus. *Cereb Cortex* 13:765–772
- Krumbholz K, Schönwiesner M, von Cramon DY, Rübsamen R, Shah NJ, Zilles K, Fink GR (2005) Representation of interaural temporal information from left and right auditory space in the human planum temporale and inferior parietal lobe. *Cereb Cortex* 15:317–324
- Lachs G, Al-Shaikh R, Bi Q, Saia RA, Teich M (1984) A neural counting model based on physiological characteristics of the peripheral auditory system. V. Applications to loudness estimation and intensity discrimination. *IEEE Trans Syst Man Cybern SMC* 14:819–836
- Lakatos P, Pincze Z, Fu KG, Javitt DC, Karmos G, Schroeder CE (2005) Timing of pure tone and noise-evoked responses in macaque auditory cortex. *NeuroReport* 16:933–937

- Langner G, Sams M, Heli P, Schulze H (1997) Frequency and periodicity are represented in orthogonal maps in the human auditory cortex: evidence from magnetoencephalography. *J Comp Physiol A* 181:665–676
- Levitt H (1971) Transformed up-down procedures in psychophysics. *J Acoust Soc Am* 49:467–477
- Licklider JCR (1951) A duplex theory of pitch perception. *Experimenta* 7:128–134
- Lindemann W (1986) Extension of a binaural cross-correlation model by means of contralateral inhibition. I: Simulation of lateralization of stationary signals. *J Acoust Soc Am* 80:1608–1622
- Lütkenhöner B, Lammertmann C, Knecht S (2001) Latency of auditory evoked field deflection N100m ruled by pitch or spectrum? *Audiol NeuroOtol* 6:263–278
- Lütkenhöner B, Krumbholz K, Seither-Preisler A (2003) Studies of tonotopy based on wave N100 of the auditory evoked field are problematic. *Neuroimage* 19:935–949
- Maeder PP, Meuli RA, Adriani M, Bellmann A, Fornari E, Thiran JP, Pittet A, Clarke S (2001) Distinct pathways involved in sound recognition and localization: a human fMRI study. *Neuroimage* 14:802–816
- McAlpine D, Grothe B (2003) Sound localization and delay lines—do mammals fit the model? *Trends Neurosci* 13:347–350
- McAlpine D, Jiang D, Palmer AR (2001) A neural code for low-frequency sound localization in mammals. *Nature Neurosci* 4:396–401
- McEvoy LK, Picton TW, Champagne SC (1991) The timing of the processes underlying lateralization: psychophysical and evoked potential measures. *Ear Hear* 12:389–398
- McEvoy L, Hari R, Imada T, Sams M (1993) Human auditory cortical mechanisms of sound lateralization: II. Interaural time differences at sound onset. *Hear Res* 67:98–109
- McPherson DL, Starr A (1993) Binaural interaction in auditory evoked potentials: Brainstem, middle- and long-latency components. *Hear Res* 66:91–98
- Meddis R, Hewitt M (1991) Virtual pitch and phase sensitivity of a computer model of the auditory periphery. I: Pitch identification. *J Acoust Soc Am* 89:2866–2882
- Mehrgardt S, Mellert V (1977) Transformation characteristics of the external human ear. *J Acoust Soc Am* 61:1567–1576
- Merthayasa IN, Hemmi H, Ando Y (1994) Loudness of a 1 kHz pure tone and sharply (1080 dB/Oct.) filtered noises centered on its frequency. *Mem Grad School Sci Tech Kobe Univ* 12A:147–156
- Mosteller F (1951) Remarks on the method of paired comparisons III. *Psychometrika* 16:207–218
- Nedzelitsky V (1980) Sound pressure in the basal turn of the cat cochlea. *J Acoust Soc Am* 68:1676–1689
- Onchi Y (1961) Mechanism of the middle ear. *J Acoust Soc Am* 21:794–805
- Osman E (1971) A correlation model of binaural masking level differences. *J Acoust Soc Am* 50:1494–1511
- Osman E, Tzuo HY, Tzuo PL (1975) Theoretical analysis of detection of monaural signals as a function of interaural noise correlation and signal frequency. *J Acoust Soc Am* 57:939–942
- Palmer AR, Jiang D, McAlpine D (1999) Desynchronizing responses to correlated noise: a mechanism for binaural masking level differences at the inferior colliculus. *J Physiol* 417:722–734
- Palomäki K, Tiitinen H, Mäkinen V, May PJC, Alku P (2005) Spatial pro-processing in human auditory cortex: the effects of 3D, ITD, and ILD stimulation techniques. *Cogn Brain Res* 24:364–379
- Pantev C, Lütkenhöner B, Hoke M, Lehnertz K (1986) Comparison between simultaneously recorded auditory-evoked magnetic fields and potentials elicited by ipsilateral, contralateral, and binaural tone burst stimulation. *Audiology* 25:54–61
- Pantev C, Hoke M, Lehnertz K, Lütkenhöner B, Anogianakis G, Wittkowski W (1988) Tonotopic organization of the human auditory cortex revealed by transient auditory evoked magnetic fields. *Electroenceph Clin Neurophysiol* 69:160–170
- Pantev C, Hoke M, Lehnertz K, Lütkenhöner B (1989) Neuromagnetic evidence of an amplitopic organization of the human auditory cortex. *Electroenceph Clin Neurophysiol* 72:225–231

- Pantev C, Bertrand O, Eulitz C, Verkindt C, Hampson S, Schuierer G, Elbert T (1995) Specific tonotopic organizations of different areas of the human auditory cortex revealed by simultaneous magnetic and electric recordings. *Electroenceph Clin Neurophysiol* 94:26–40
- Patterson RD, Allerhand M, Giguere C (1995) Time-domain modelling of peripheral auditory processing: A modular architecture and a software platform. *J Acoust Soc Am* 98:1890–1894
- Pickles JO (1983) Auditory-nerve correlates of loudness summation with stimulus bandwidth, in normal and pathological cochleae. *Hear Res* 12:239–250
- Pickles JO (ed) (2008) An introduction to the physiology of hearing, 3rd edn. Academic Press, London
- Puria S, William T, Peake WT, Rosowski JJ (1997) Sound-pressure measurements in the cochlear vestibule of human-cadaver ears. *J Acoust Soc Am* 101:2754–2770
- Rauschecker JP, Tian B (2000) Mechanisms and streams for processing of “what” and “where” in auditory cortex. *Proc Natl Acad Sci USA* 97:11800–11806
- Rauschecker JP, Tian B, Hauser M (1995) Processing of complex sounds in the macaque nonprimary auditory cortex. *Science* 268:111–114
- Reite M, Zimmerman JT, Edrich J, Zimmerman JE (1982) Auditory evoked magnetic fields: response amplitude vs. stimulus intensity. *Electroenceph Clin Neurophysiol* 54:147–152
- Relkin EM, Doucet JR (1997) Is loudness simply proportional to the auditory nerve spike count? *J Acoust Soc Am* 101:2735–2740
- Roberts TPL, Poeppel D (1996) Latency of auditory evoked M100 as a function of tone frequency. *NeuroReport* 7:1138–1140
- Romani GL, Williamson SJ, Kaufman L (1982) Tonotopic organization of the human auditory cortex. *Science* 216:1339–1340
- Rubinstein M, Feldman B, Fischler F, Frei EH, Spira D (1966) Measurement of stapedial-footplate displacements during transmission of sound through the middle ear. *J Acoust Soc Am* 44:1420–1426
- Rylander R, Björkman M (1997) Annoyance by aircraft noise around small airports. *J Sound Vib* 205:533–538
- Rylander R, Sörensen S, Kajland A (1972) Annoyance reactions from aircraft noise exposure. *J Sound Vib* 24:419–444
- Rylander R, Björkman M, Åhrlin U, Sörensen S, Kajland A (1980) Aircraft noise contours: importance of overflight frequency and noise level. *J Sound Vib* 69:583–595
- Rylander R, Björkman M, Åhrlin U, Arntzen U, Solberg S (1986) Dose–response relationships for traffic noise and annoyance. *Arch Environ Health* 41:7–10
- Saberi K, Takahashi Y, Konishi M, Albeck Y, Arthur BJ, Farahbod H (1998) Effects of interaural decorrelation on neural and behavioral detection of spatial cues. *Neuron* 21:789–798
- Sams M, Hämäläinen M, Hari R, McEvoy L (1993) Human auditory cortical mechanisms of sound lateralization: I. Interaural time differences within sound. *Hear Res* 67:89–97
- Sato S, Kitamura T, Ando Y (2002) Loudness of sharply (2068 dB/Octave) filtered noises in relation to the factors extracted from the autocorrelation function. *J Sound Vib* 250:47–52
- Sato S, Nishio K, Ando Y (2003) Propagation of alpha waves corresponding to subjective preference from the right hemisphere to the left with changes in the IACC of a sound field. *J Temporal Des Arch Environ* 3:60–69
- Scharf B (1962) Loudness summation and spectrum shape. *J Acoust Soc Am* 34:228–233
- Schlauch RS, Wier CC (1987) A method for relating loudness matching and intensity discrimination data. *J Speech Hear Res* 30:13–20
- Secker-Walker HE, Searle C (1990) Time domain analysis of auditory-nerve-fiber firing rates. *J Acoust Soc Am* 88:1427–1436
- Seither-Preisler A, Krumbholz K, Lutkenhoner B (2003) Sensitivity of the neuromagnetic N100m deflection to spectral bandwidth: A function of the auditory periphery? *Audiol Neurotol* 8:322–337
- Seither-Preisler A, Krumbholz K, Patterson RD, Seither S, Lutkenhoner B (2004) Interaction between the neuromagnetic responses to sound energy onset and pitch onset suggests common generators. *Eur J Neurosci* 19:3073–3080

- Shackleton TM, Arnott RH, Palmer AR (2005) Sensitivity to interaural correlation of single neurons in the inferior colliculus of guinea pigs. *J Assoc Res Otolaryngol* 6:244–259
- Shaw EAG (1974) Transformation of sound pressure level from the free field to the eardrum in the horizontal plane. *J Acoust Soc Am* 56:1848–1861
- Shaw EAG, Teranishi R (1968) Sound pressure generated in an external-ear replica and real human ears by a nearby point source. *J Acoust Soc Am* 44:240–249
- Shofner WP (1991) Temporal representation of rippled noise in the anteroventral cochlear nucleus of the chinchilla. *J Acoust Soc Am* 90:2450–2466
- Shofner WP (1999) Responses of cochlear nucleus units in the chinchilla to iterated rippled noises: analysis of neural autocorrelograms. *J Neurophysiol* 81:2662–2674
- Soeta Y, Nakagawa S (2008a) The effect of pitch and pitch strength on an auditory-evoked N1m. *NeuroReport* 19:783–787
- Soeta Y, Nakagawa S (2008b) Relationship between loudness and auditory evoked N1m. *Interdisci Res Explor, Biomagnetism*, pp 95–97
- Soeta Y, Nakagawa S (2009) Level-dependent growth on auditory evoked N1m for low- and high-frequency tones. *NeuroReport* 20:548–552
- Soeta Y, Nakagawa S, Tonoike M, Ando Y (2002) Magnetoencephalographic responses corresponding to individual subjective preference of sound fields. *J Sound Vib* 258:419–428
- Soeta Y, Nakagawa S, Tonoike M, Ando Y (2003) Spatial analyses of magnetoencephalographic activities in relation to subjective preference of a sound field. *J Temporal Des Arch Environ* 3:28–35
- Soeta Y, Maruo T, Ando Y (2004a) Annoyance of bandpass filtered noises in relation to the factor extracted from autocorrelation function. *J Acoust Soc Am* 116:3275–3278
- Soeta Y, Hotehama T, Nakagawa S, Tonoike M, Ando Y (2004b) Auditory evoked magnetic fields in relation to the inter-aural cross-correlation of bandpass noise. *Hear Res* 96:109–114
- Soeta Y, Nakagawa S, Tonoike M, Ando Y (2004c) Magnetoencephalographic responses corresponds to individual annoyance of bandpass noise. *J Sound Vib* 277:479–489
- Soeta Y, Nakagawa S, Tonoike M (2005a) Auditory evoked magnetic fields in relation to bandwidth variations of bandpass noise. *Hear Res* 202:47–54
- Soeta Y, Nakagawa S, Tonoike M (2005b) Auditory evoked magnetic fields in relation to the iterated rippled noise. *Hear Res* 205:256–261
- Soeta Y, Nakagawa S, Matsuoka K (2006) The effect of center frequency and bandwidth on the auditory evoked magnetic field. *Hear Res* 218:64–71
- Stecker GC, Harrington IA, Middlebrooks JC (2005) Location coding by opponent neural populations in the auditory cortex. *PLoS Biol* 3:520–528
- Stufflebeam SM, Poeppel D, Rowley HA, Roberts TPL (1998) Peri-threshold encoding of stimulus frequency and intensity in the M100 latency. *NeuroReport* 9:91–94
- Suzuki Y, Takeshima H (2004) Equal-loudness counters for pure tones. *J Acoust Soc Am* 116:918–933
- ten Kate JH, van Bakkum MF (1988) Synchrony-dependent autocorrelation in eighth-nerve-fiber response to rippled noise. *J Acoust Soc Am* 84:2092–2102
- Thurstone LL (1927) A law of comparative judgement. *Psychol Rev* 34:273–289
- Tiihonen J, Hari RM, Kajola M, Karhu J, Ahlfors S, Tisari S (1991) Magnetoencephalographic 10-Hz rhythm from the human auditory cortex. *Neurosci Lett* 129:303–305
- Vasama JP, Mäkelä JP, Tisari SO, Hämäläinen MS (1995) Effects of intensity variation on human auditory evoked magnetic fields. *Acta Otolaryngol (Stockh)* 115:616–621
- Wada H, Metoki T, Kobayashi T (1992) Analysis of dynamic behavior of human middle-ear using a finite-element method. *J Acoust Soc Am* 92:3157–3168
- Wessinger CM, VanMeter J, Tian B, Van Lare J, Pekar J, Rauschecker JP (2001) Hierarchical organization of the human auditory cortex revealed by functional magnetic resonance imaging. *J Cogn Neurosci* 13:1–7
- Wiener FM, Ross DA (1946) The pressure distribution in the auditory canal in a progressive sound field. *J Acoust Soc Am* 18:401–408
- Wightman FL (1973) The pattern-transformation model of pitch. *J Acoust Soc Am* 54:407–416

- Winter IM, Wiegand L, Patterson RD (2001) The temporal representation of the delay of iterated rippled noise in the ventral cochlear nucleus of the guinea-pig. *J Physiol* 537:553–566
- Woldorff MG, Tempelmann C, Fell J, Tegeler C, Gaschler-Markefski B, Hinrichs H, Heinze H, Scheich H (1999) Lateralized auditory spatial perception and the contralaterality of cortical processing as studied with functional magnetic resonance imaging and magnetoencephalography. *Hum Brain Mapp* 7:49–66
- Yin TC, Chan JC (1990) Interaural time sensitivity in medial superior olive of cat. *J Neurophysiol* 64:465–488
- Yin TC, Chan JCK, Carney LH (1987) Effects of interaural time delays of noise stimuli on low-frequency cells in the cat's inferior colliculus. III. Evidence for cross-correlation. *J Neurophysiol* 58:562–583
- Yost WA (1996) Pitch strength of iterated rippled noise. *J Acoust Soc Am* 100:3329–3335
- Yost WA (ed) (2000) Fundamentals of hearing: an introduction. Academic Press, San Diego
- Yost WA, Hill R (1979) Models of the pitch and pitch strength of ripple noise. *J Acoust Soc Am* 66:400–410
- Yost WA, Patterson R, Sheft S (1996) A time domain description for the pitch strength of iterated ripple noise. *J Acoust Soc Am* 99:1066–1078
- Yvert B, Bertrand O, Pernier J, Ilmoniemi RJ (1998) Human cortical responses evoked by dichotically presented tones of different frequencies. *NeuroReport* 9:1115–1119
- Zimmer U, Macaluso E (2005) High binaural coherence determines successful sound localization and increased activity in posterior auditory areas. *Neuron* 47:893–905
- Zwicker E, Flottorp G, Stevens SS (1957) Critical bandwidth in loudness summation. *J Acoust Soc Am* 29:548–557
- Zwislocki JJ (1962) Analysis of middle ear function. Part I: input impedance. *J Acoust Soc Am* 35:1514–1523
- Zwislocki JJ (1965) Analysis of some auditory characteristics. *Handb Math Psychol* 3:1–97

Neurally Based Measurement and Evaluation of
Environmental Noise

Soeta, Y.; Ando, Y.

2015, XII, 264 p. 184 illus., Hardcover

ISBN: 978-4-431-55431-8